Navigating uncertainty and sensitivity analysis of future tropical cyclone risk estimates

Simona Meiler[1,2,*], Chahan M. Kropf[1,2], Jamie W. McCaughey[1,2], Chia-Ying Lee[3], Suzana J. Camargo[3], Adam H. Sobel[3,4], Nadia Bloemendaal[5,6], Kerry Emanuel[7], and David N. Bresch[1,2]

[1]Institute for Environmental Decisions, ETH Zurich, Switzerland
[2]Federal Office of Meteorology and Climatology MeteoSwiss, Switzerland
[3]Lamont-Doherty Earth Observatory, Columbia University, Palisades, NY, USA
[4]Department of Applied Physics and Applied Mathematics, Columbia University, New York, NY, USA
[5]Institute for Environmental Studies (IVM), Vrije Universiteit Amsterdam, Amsterdam, The Netherlands
[6]Royal Netherlands Meteorological Institute, De Bilt, The Netherlands
[7]Lorenz Center, Massachusetts Institute of Technology, Cambridge, Massachusetts, USA
[*]Corresponding author: simona.meiler@usys.ethz.ch

This manuscript is a non-peer reviewed preprint submitted to Science Advances. Please note that the manuscript is currently under review and has not yet been accepted for publication. Subsequent versions of this manuscript may have different content. If accepted, the final version of this manuscript will be available via the 'Peer reviewed Publication DOI' link on its EarthArXiv web page. Please feel free to contact us with any comments or feedback about our study.

ABSTRACT

Future tropical cyclone risks will evolve depending on climate change and socio-economic development, entailing significant uncertainties. An uncertainty and sensitivity analysis of future tropical cyclone risks is thus vital for robust decision-making and model improvement. However, the outcomes of such uncertainty and sensitivity analyses are tied to the chosen model setup, warranting caution in interpretation and extrapolation. Our study investigates how four distinct tropical cyclone hazard models and alternate representations of socio-economic development influence future tropical cyclone risk. We find that average tropical cyclone risk will increase 1-5% by 2050 across all models and global study regions. The estimated maximum risk increases by 2100, in contrast, ranging from 10-400% depending on the hazard model choice. The dominant source of uncertainty in these risk estimates changes with the specific risk model setup. Finally, we differentiate between aleatory, epistemic, and normative uncertainties, offering guidance to reduce these uncertainties and provide better-informed decision-making.

Teaser

Quantifying, classifying and comparing uncertainties in future tropical cyclone risks towards actionable climate decisions.

1 Introduction

In recent years, catastrophe modelling has expanded beyond its traditional realm in the (re-)insurance industry to serve the broader global financial market, and has also found increasing applications to humanitarian and sustainable development efforts. As climate change is represented in the models used, we refer to them broadly as climate risk models, a category that includes, but is broader than, the catastrophe models that have a longer history in (re-)insurance. Many consultancies, financial technology firms, data providers, and investment advisory groups now offer information about localized physical climate risks, entering a technology arms race among climate services providers (1, 2). However, the proprietary nature of their products inhibits both transparency and accessibility, and makes it difficult to evaluate or compare them (1–3). Efforts to establish measurement and reporting standards are still evolving (4). Beyond insurance and finance, climate risk modelling is also increasingly being applied to inform adaptation decisions in development and humanitarian programs, where the potential for societal benefit is large (5, 6). Here too, there is a pressing need for a better understanding of the quality and reliability of climate risk assessments (7, 8).

Tropical cyclone (TC) risk provides a prime example of the challenges and complexities faced in the broader field of climate risk analysis. TCs are among the most destructive of natural hazards, posing significant threats to people (9) and assets (10) exposed to these events. In the future, TC risks are expected to increase further due to the warming climate and socio-economic development (9, 11, 12). It is thus crucial to support at-risk communities with reliable and transparent TC risk assessments. However, providing reliable TC risk assessment is challenging due to uncertainties in the model input components and model structure (13). TC risks emerge from the interplay of TC hazards, the extent to which people and assets are exposed to these hazards, and the vulnerability of the exposed individuals and the (built) environment to these hazards (14). Each of these risk elements is subject to numerous uncertainties, and additional uncertainty emerges when they are combined. Meiler et al. (2022) (15) investigate uncertainties in the TC hazard model choice for present-day loss estimates. Assessing future TC risks requires additional modelling choices regarding the representation of future climate and socio-economic systems. Each of those introduces its own uncertainties and is further confounded by the lack of verification data (16, 17).

This study distinguishes three types of uncertainty - epistemic, aleatory, and normative - that are relevant to climate risk assessment, extending beyond the scope of TCs. Epistemic uncertainty arises from limited knowledge about the systems being modelled, and involves the structural uncertainties in synthetic TC models, historical data quality, and understanding of environmental interactions (18). It includes scenario uncertainty, i.e., the unpredictability of future emissions scenarios (19–22), and model uncertainty (19–21), which here, for example, refers to the limitations of climate models, models used to generate synthetic TCs, or the exposure model to derive a spatially explicit map of asset values. Aleatory uncertainty stems from the inherent randomness of natural processes, such as climate variability that is internal or unforced by human influence (18). This type of uncertainty can be quantified through statistical methods, like Monte Carlo simulations, to estimate the probability distribution of outcomes. Normative uncertainty emerges from subjective decisions and ethical considerations in risk assessment processes, influencing the choice of valuation units and risk metrics (23–25). While not quantifiable like epistemic or aleatory uncertainties, normative uncertainty can be addressed through increased transparency, stakeholder engagement, and the integration of diverse ethical perspectives (26).

Given the complexities of epistemic, aleatory, and normative uncertainties, a systematic approach to uncertainty quantification emerges as a critical need. In this study, we utilize the uncertainty and sensitivity quantification (unsequa) module (13), a tool already integrated within the risk modelling platform CLIMADA (27), which allows for uncertainty and sensitivity analyses of all CLIMADA-based risk calculations. We systematically quantify uncertainties and sensitivities in future TC risk change estimates in the middle and at the end of the century, encompassing uncertainties in all risk model components: hazard, exposure, and vulnerability. Contrasting results from two previous studies assessing uncertainties and sensitivities in the quantification of future TC risks, each using a different TC hazard model, show that the results of such uncertainty and sensitivity quantification depend on the scope of the study, which is defined a priori by investigator choice - in other words, uncertainty assessment is itself uncertain (16, 28, 29).

Hence, in this study, we further investigate the uncertainty in estimated future TC risk that arises not only from the choice of hazard models, but also from alternative representations of socio-economic development. For the hazard, we use four different, global-scale, academic models, differing in structure and approach, to generate different future TC event sets. These models are used to downscale multiple emission scenarios and climate models for two future periods. Specifically, we contrast TC event sets from two statistical-dynamical TC models, the MIT model (30, 31) and Columbia HAZard model (CHAZ) (32, 33), the fully statistical model STORM (34, 35) and a more simplistic, statistical model (IBTrACS_p) applying a random walk algorithm (12, 36) to historical TC observations from the International Best Track Archive for Climate Stewardship (IBTrACS) (37). Furthermore, we use economic growth factors from various Shared Socioeconomic Pathways (SSPs) (38) to approximate and analyze socio-economic development, thereby addressing growth uncertainties in future exposure. We consider all five SSP scenarios, which describe diverse future societal trajectories. These scenarios are informed by GDP projections from three distinct research institutions (OECD (39), IIASA (40), PIK (41)), each providing alternative interpretations of economic development under the SSP framework. We do not speculate on future changes in the vulnerability function due to the current knowledge gap in this matter. Instead, we explore uncertainties by adjusting the slope parameter of regionally-calibrated vulnerability functions based on historical data (42) within a wide range. We perform the uncertainty and sensitivity analysis for future TC risk change estimates based on all possible combinations of input factors, relying on a numerical Quasi-Monte Carlo scheme (43) to repeat the risk calculation many times ($>$20 000). A schematic overview of the uncertainty and sensitivity analysis conducted in this study is shown in Figure 1.

While previous studies have examined how variations in hazard, exposure, and vulnerability translate into risk, this is the first study to include four distinct hazard models (and variations of these) in such an analysis. Hence, this study thus offers new insights into the structural differences between TC models and their implications for risk assessment. We synthesize aspects of model choice, model complexity, and their implication for uncertainty and sensitivity analysis of future TC risk models.

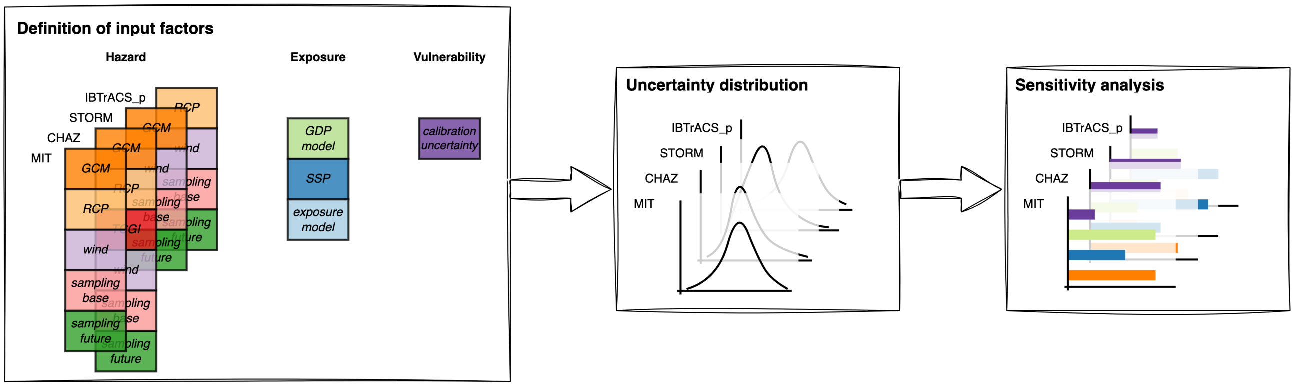

Fig. 1. Schematic overview of uncertainty and sensitivity analysis. The definition of input factors depicts which risk model input components are varied (left-most box); the characterization of their variability space is detailed in Section 4.8. Input factors pertaining to the hazard are defined for each TC model (MIT; CHAZ, STORM, IBTrACS_p) separately. The risk calculation is repeated (>20 000) times for all possible combinations of input factors yielding an uncertainty distribution for the risk model setup for each TC model (middle box). Sensitivity indices are calculated from these distributions (right-most box).

2 Results

2.1 Drivers of future TC risk change across hazard models

Future TC risks change due to both the warming climate and socio-economic development. Here, we first evaluate the individual contributions of these two key drivers to future TC risk estimates across hazard models. To consider the influence of climate change on risk, we hold exposure constant at a reference state while using varying future climate hazard representations. Conversely, to assess the impact of socio-economic factors, we keep the hazard data fixed at the present-day baseline, allowing socio-economic conditions to vary. Then, we study future TC risk change estimates of both key drivers acting together. TC risks are expressed by the common metric of expected annual damage (EAD) and 100-yr damage event (100-yr event in short), reported as relative changes (in %) compared to present-day baselines. We present results for four study regions: North Atlantic/Eastern Pacific, North Indian Ocean, Southern Hemisphere, and North Western Pacific (see Methods 4.1). We limit the results' description to the EAD in this section because the corresponding key findings for the 100-yr event are comparable (cf. Supplementary Fig. 1).

Climate change generally affects the median TC risk changes comparably across hazard models, study regions and periods (Fig. 2, left-most boxplots in all panels). Specifically, the median change in EAD is usually on the order of 0 % to −1 %. However, the uncertainty in TC risk change estimates is notably higher for all MIT hazard results than the other hazard model outputs, as can be derived from the width of the interquartile range of the boxplots shown in Figure 2. Furthermore, maximum values for climate change-driven EAD increase from the MIT hazard reach 20% (45%), 19% (28%), 6% (8%), and 14% (14%) in the North Atlantic/Eastern Pacific, North Indian Ocean, Southern Hemisphere, and Western Pacific in the middle (at the end) of the century. In contrast, maximum risk increases from the other hazard models do not exceed the 5%-mark except in the North Indian Ocean. There, climate change raises EAD values from CHAZ by 10% (9%) and IBTrACS_p by 23% (23%) in 2050 (2090), respectively. Only the results from STORM remain low due to known high-intensity biases in the reference period hazard set (15, 29). The North Indian Ocean is, furthermore, the region where uncertainties in climate-driven risk change are highest across all hazard models. Additionally, median TC risk changes are lowest in the Southern Hemisphere over all regions, including negative values for CHAZ and IBTrACS_p. In other words, climate-driven TC risk decreases in these cases. Indeed, we find negative minima of ca. 0 % to −1 % for all hazard models and regions.

Socio-economic development emerges as the predominant driver for TC risk increase, as can be seen from the greater increase in risk associated with socio-economic development alone than with climate change alone (Fig. 2). This is consistent across all hazard models, using the same future socio-economic representation for each. Notably, any difference between the hazard models stems primarily from their distinct present-day baseline. Specifically, the median EAD changes driven by socio-economic development are around 1 % to 2 % by 2050. In regions like the North Atlantic/Eastern Pacific and Western Pacific, this is roughly double the changes attributed to climate change. However, in the North Indian Ocean, median values are higher: 2.5 % to 3 % (and 6 % to 7 % by 2050 (2090), which is about four times the climate change contributions. Furthermore, the uncertainty tied to socio-economic development is most pronounced in the Southern Hemisphere across regions. Finally, when considering the hazard sets CHAZ, STORM, and IBTrACS_p, socio-economic development presents more uncertainty than climate change. In contrast, for MIT-based calculations, climate change is the more uncertain risk driver.

Next, we assess the total TC risk increase, factoring in both climate change and socio-economic development. Notably, the total TC risk increase, as depicted in Figure 2 (total; right-most column), are not simple sums or products of risk increases attributed only to climate change or only to socio-economic development, suggesting some further interdependencies between these drivers, (Fig. 2 (sum; inner right column)).

Median EAD raises by 0.9% (CHAZ) to 2.3% (MIT), 2.1% (STORM) to 5.3% (MIT), 1.1% (IBTrACS_p) to 3.8% (MIT), and 1.4% (CHAZ) to 3.8% (MIT) in the North Atlantic/Eastern Pacific, North Indian Ocean, Southern Hemisphere, and Western Pacific by 2050. In all regions, the median risk increase is highest for the MIT hazard, while the other three models tend to cluster around similar values, with STORM producing slightly higher results in the Southern Hemisphere and Western Pacific than CHAZ and IBTrACS_p. By the end of the century, the median risk increases further, reaching levels approximately two to three times the increase in EAD estimated for 2050. Furthermore, maximum total EAD increases by 2090 span from 11% (CHAZ) to 264% (MIT), 134% (CHAZ) to 393% (MIT), 22% (IBTrACS_p) to 159% (MIT), and 15% (CHAZ) to 96% (MIT) in the North Atlantic/Eastern Pacific, North Indian Ocean, Southern Hemisphere, and Western Pacific respectively, highlighting the significant uncertainty in these results. We focus on total risk increases for the remainder of the study as described in this last paragraph.

2.2 Uncertainty of future TC risk change across hazard models

To quantify uncertainty in future TC risk change estimates, we calculate a probability distribution of outcomes across all combinations of input factors within four distinct model setups for each TC hazard model. Here, we analyze these output distributions of risk change estimates (Fig. 3). We present the main findings for uncertainties of future TC risk change, focusing on changes in EAD, consistent with the preceding section. For results of the 100-yr event, which are comparable., see Supplementary Fig. 2.

Figure 3 presents the probability density distributions of the total TC risk change, derived from the same data as the boxplots (total) in Figure 2. We identify density peaks of EAD change for CHAZ, STORM, and IBTrACS_p hazard sets in each region and both future periods around 1 % to 3 %. The density distributions from the MIT model, however, peak at higher values, consistent with the assessment of median total TC risk change from the previous section. Interestingly, when considering both risk metrics - EAD (Fig. 3) and the 100-yr event (Supplementary Fig. 2) - we observe that their density distributions peak at very similar values for each combination of region, year, and hazard model (Supplementary Table 1). This consistency suggests that socio-economic development is the predominant driver for total TC risk change, influencing the magnitude and peak of the density distribution. Consequently, the choice between the two risk metrics does not significantly affect this outcome. Any differences between these metrics are predominantly shaped by the hazard, making them secondary in this context.

Conversely, when examining the entire probability density distribution, the MIT results display a notably broader distribution compared to the other three hazard sets, a finding consistent with results from Figure 2. The width of a distribution can serve as an indication of its associated uncertainty. Drawing from insights in the previous section, the width of the MIT-based distribution can be interpreted as an imprint of the uncertainties associated with climate change as a more uncertain risk driver. In contrast, the similar shapes of distributions from CHAZ, STORM, and IBTrACS_p models indicate socio-economic development as their main source of uncertainty, as corroborated by Figure 2. Furthermore, we observe wider distributions for results in 2090 compared to 2050 for all hazard models, related to increasing uncertainty in time. While this analysis provides insights into the overarching uncertainty, a more detailed examination of individual input factors is essential. In the following section, we explore these factors in detail through a sensitivity analysis.

2.3 Sensitivity of future TC risk change across hazard models

Sensitivity analysis helps identify and quantify the relative importance of individual input factors for the output uncertainty of future TC risk change estimates described in the last section. The model input factors and their parameter ranges are defined to capture the inherent uncertainties in the different components related to the representation of future TC hazards, exposure, and vulnerability. Here, we present first-order and total-order Sobol sensitivity indices (44, 45) to assess the impact of the input factors on our TC risk change calculations across the four hazard models. First-order sensitivity indices measure the effect of variations in a single input factor. They are often used to rank the input factors according to their relative contribution to the output variability (ranking). Total-order indices evaluate the cumulative effect, considering all factors and their potential interactions. They are commonly used for screening, aiming to identify the input factors - if any - with negligible influence on the output variability (46). We note that not all hazard models encompass all input factors (Methods 4.8).

The highest sensitivity indices describe the dominant source of uncertainty for future TC risk changes, which varies between the different hazard models. In the MIT model-based analyses, the highest sensitivity index stems from the choice of GCM

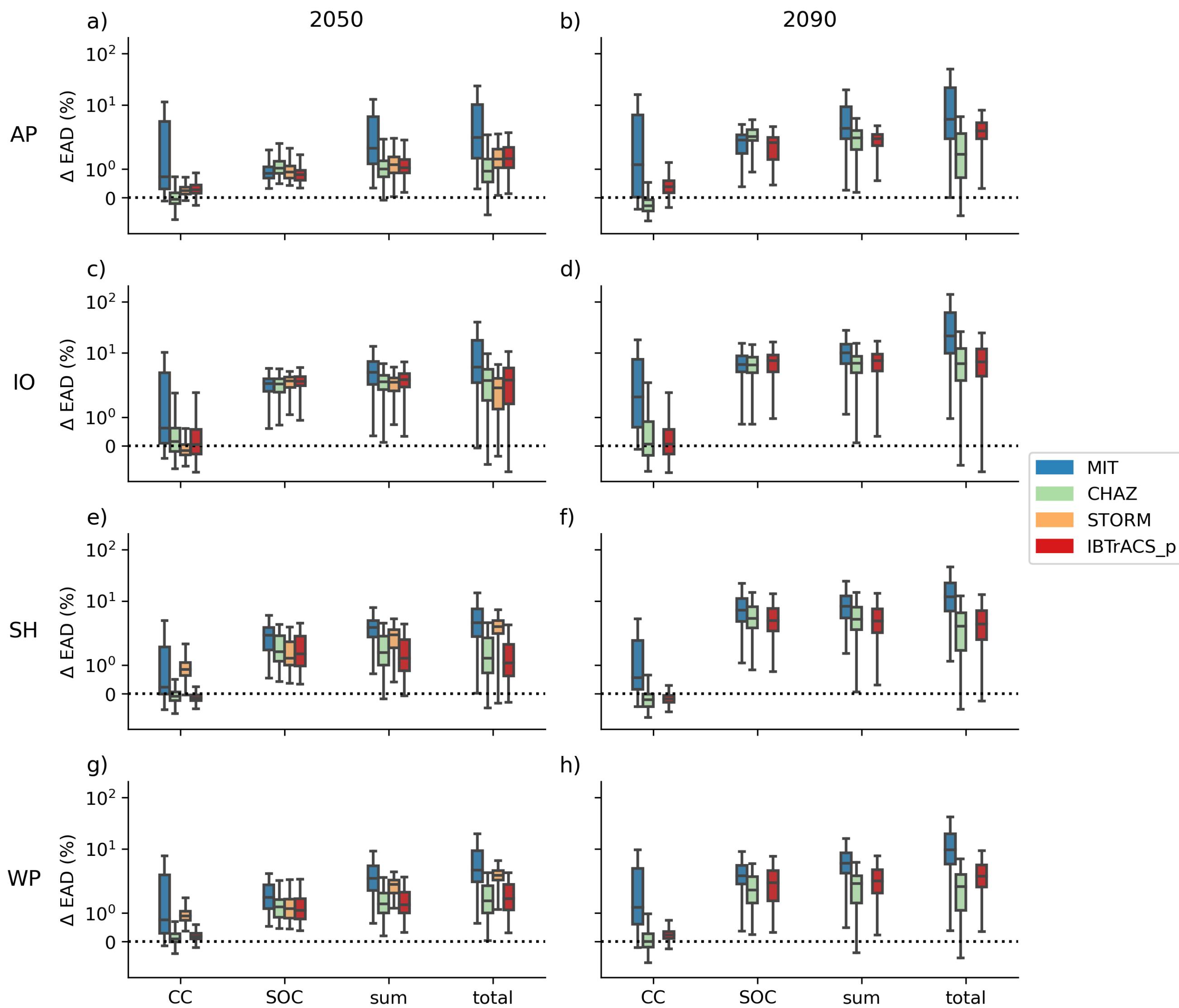

Fig. 2. Drivers of future tropical cyclone risk change across hazard models. Relative change in expected annual damage (EAD) by 2050 (left panels) and 2090 (right panels) due to climate change (CC), socio-economic development (SOC), the product of CC and SOC calculated from the sum of their log values (sum) and both drivers interacting (total) with respect to the historical baseline. The relative change EAD is reported for the four study regions (North Atlantic/Eastern Pacific (AP), North Indian Ocean (IO), Southern Hemisphere (SH), and North Western Pacific (WP)). Boxplots are shown for the four models MIT (blue), CHAZ (green), STORM (orange), IBTrACS_p (red) and display the interquartile range (IQR) for the uncertainty over all input factors (see Methods), while the whiskers extend to 1.5 times the IQR. More extreme points (outliers) are not shown. Note that STORM results are only available for 2050. Note the mirrored logarithmic scale on the y-axis.

used in downscaling TC events sets (*GCM*) (Fig. 4 a), e)). Conversely, the SSP-based scaling of the exposure points (*SSP exposure*) generally exhibits the largest sensitivity for all other hazard models. Specifically, this holds for most results in the Southern Hemisphere and Western Pacific for the CHAZ, STORM and IBTrACS_p and both future periods. In the North Indian Ocean, sensitivity indices are highest for input factors related to the hazard component *GCM, TCGI moisture variable, Event subsampling base/future*, and results in the North Atlantic/Eastern Pacific follow no consistent trend beyond the primary observations mentioned. A detailed compilation of the most significant sensitivity indices for future TC risk estimates can be found in Supplementary Table 2.

Moreover, the sensitivity analysis reveals several distinctive patterns. First, the GCM choice (*GCM*) is more important in the North Atlantic/Eastern Pacific, North Indian Ocean, and Western Pacific than in the Southern Hemisphere for the three hazard

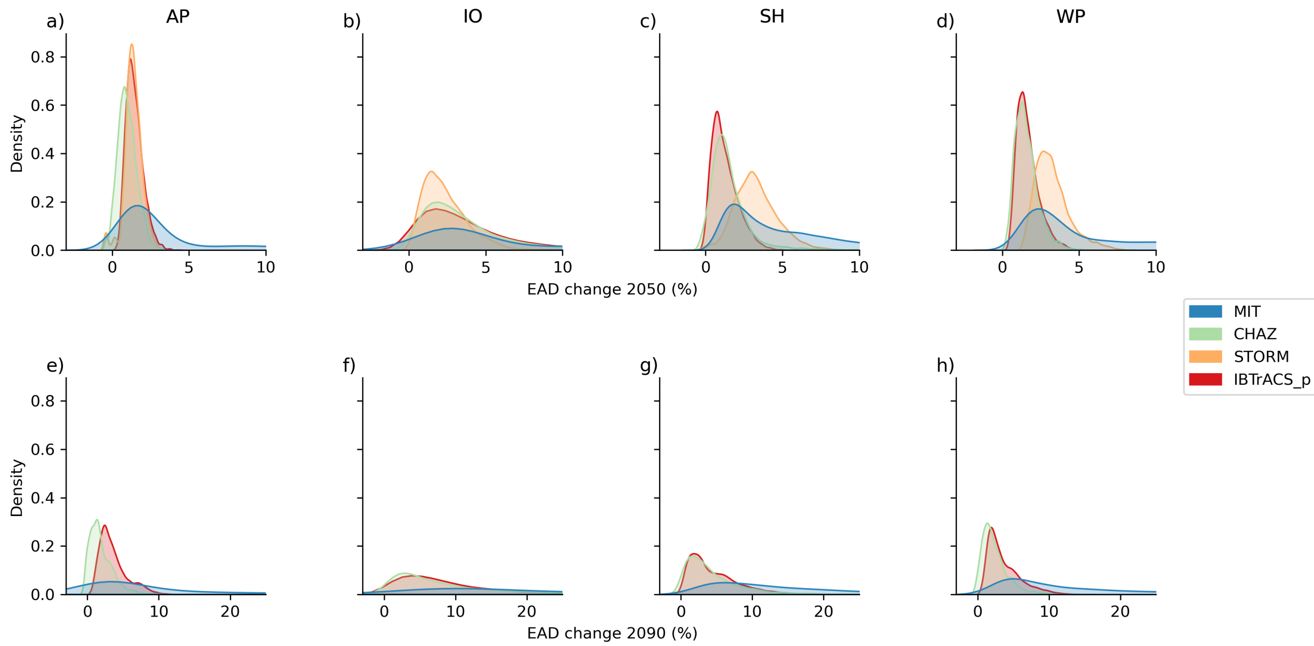

Fig. 3. Uncertainty distribution of TC risk change across hazard models. Kernel density estimation plots showcasing the uncertainty distribution of estimated relative change in expected annual damage (EAD) across study regions (North Atlantic/Eastern Pacific (AP), North Indian Ocean (IO), Southern Hemisphere (SH), and North Western Pacific (WP)) for the years 2050 and 2090. Each subplot represents a specific region and year combination, with different models (MIT, CHAZ, STORM, IBTrACS_p) depicted in distinct colors. Note, the model STORM only provides data for 2050. Each plot shows a normalized probability distribution with an integral sum of 1. The x-axis is truncated in some figures, potentially influencing the interpretation of distribution tails, particularly for the MIT hazard-based results.

models (MIT, CHAZ, STORM), which encompass this input factor. This pattern largely aligns with regions where uncertainties in climate change as a risk driver exceed uncertainties from socio-economic development (see Fig. 2). Furthermore, the GCM choice is more important for changes in EAD than in the 100-yr event. Second, for CHAZ model-based sensitivity analyses, the moisture variable within the TC genesis index (*TCGI*) is mostly of equal importance for the TC risk change uncertainty as the GCM choice (*GCM*) (Fig. 4 b), f)). Third, the variability in event subsampling for baseline and future hazard sets (*Event subsampling base/future*) is most pronounced in the IBTrACS_p-related result (Fig. 4 b), g)), in contrast to the other hazard models.

Next, we evaluate the total-order sensitivity indices (total effects) across the four hazard models. Namely, total effects are notably increased for CHAZ hazard-based results compared to their first-order indices, meaning that this model setup encompasses many interactions between input factors (Supplementary Fig. 3). In contrast, total-order sensitivity indices broadly mirror the ranking and distribution of the first-order indices for MIT- and STORM-related results. Moreover, in the IBTrACS_p-based sensitivity analysis, total effects include influences from the wind model choice (*wind model*), a nearly irrelevant factor in all other hazard sets.

Finally, we emphasize that sensitivity analysis is always specific to the choice of risk metric. To illustrate this, we show the implications of assessing TC risk in absolute terms versus changes relative to a baseline. For absolute TC risk estimates, the primary source of uncertainty across all hazard models is the input factor associated with the vulnerability function (*Vulnerability function midpoint*), as depicted in Supplementary Fig. 4 and Supplementary Fig. 5 and first discussed by Meiler et al. (2023) (28). Thus while the choice of vulnerability function is highly influential on the total risk that we calculate, this influence is much less apparent when we compare changes in risk calculated with the same vulnerability function.

3 Discussion

Our results show that while both climate change and socio-economic development influence TC risk changes, socio-economic factors are the predominant drivers of median increased risk across all hazard models. While studying these drivers in

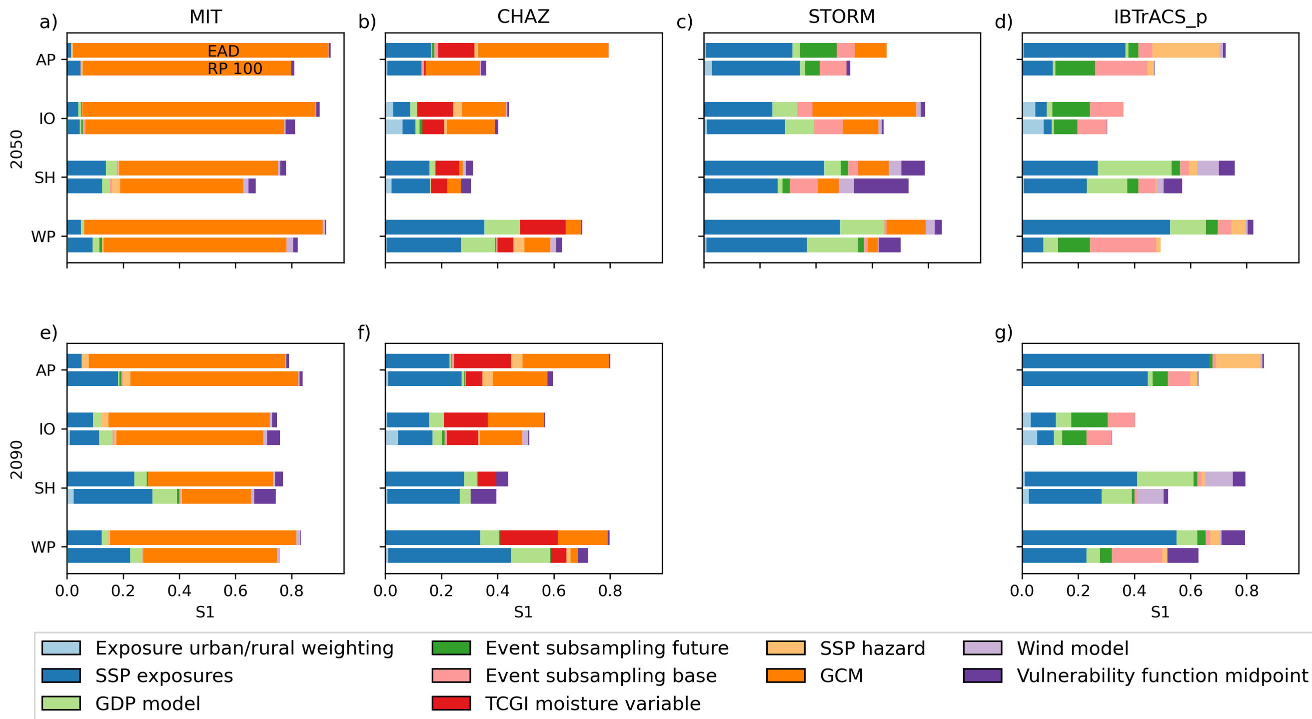

Fig. 4. Sensitivity indices of future TC risk change across hazard models. First-order Sobol sensitivity indices for future (2050, 2090) TC risk change calculated with the four models (MIT, CHAZ, STORM, IBTrACS_p), expressed as %-change in expected annual damage (EAD; upper bar for each hazard model, time, and region) and 100-yr event values (RP 100; lower bar for each hazard model, time, and region) over the four study regions (North Atlantic/Eastern Pacific (AP), North Indian Ocean (IO), Southern Hemisphere (SH), and North Western Pacific (WP)) and all input factors (different colors); *Vulnerability function midpoint* describes the impact function; *Wind model*; *GCM*, *SSP hazard*, *TCGI moisture variable*, *Event subsampling base*, *Event subsampling future* pertain to the hazard component; *GDP model*; *SSP exposure*, *Exposure urban/rural weighting* relate to the exposure. Note that STORM results are only available for 2050. Note that certain input factors apply to only one or a subset of models, c.f. Table 1.

isolation provided distinct insights, their combined effects reveal non-trivial interactions. This suggests that simply summing or multiplying their individual effects may not fully capture the complexity of their combined impact on TC risk, nor the nuances in the uncertainty and sensitivity analysis of these risk estimates. It underscores the importance of integrating both drivers from the onset in risk assessments to ensure a comprehensive understanding.

We report that median TC risk increases 1-5% by 2050 across all models and global study regions, perhaps a small enough change to be considered indistinguishable from zero for some purposes. However, the estimated maximum risk increases by the end of the century range from 10-400% depending on the hazard model choice. To the extent that we cannot rule out either any particular hazard model or any socioeconomic scenario, this suggests a much less optimistic view, with the potential for large increases in risk. Furthermore, we consider TC wind risk only and do not include the potentially compounding effects of growing TC rainfall rates, storm surge heights, and sea level rise (47). These factors likely exacerbate future TC risk increases further.

Hazard model-specific findings

For TC risk estimates based on the MIT model, climate change is the more uncertain risk driver than socio-economic development (Fig. 2), and the choice of climate model (*GCM*) dominates the output uncertainty (Fig. 4). Conversely, when using STORM, CHAZ, or IBTrACS_p, socio-economic development is the more uncertain risk driver than climate change, and the SSP-based exposure scaling (*SSP exposure*) has the highest sensitivity index. This difference is particularly notable when contrasting results from the two statistical-dynamical TC hazard models CHAZ and MIT. In a previous study solely based on MIT TC hazards, we discovered a positive relationship between the climate sensitivity of GCMs used to downscale TCs and the corresponding increase in TC risk (28). This increase is linked to the scaling of TC potential intensity with global warming (48), which in turn is a strong predictor for TC genesis potential indices (49–51). These indices again influence TC hazard frequencies and intensities, which are critical characteristics for TC risk assessment. Given the similar TC modelling approach to the MIT model, we expected to find a comparable relationship in the CHAZ-based results. Surprisingly, we found no striking relationship between transient climate response (TCR; Supplementary Table 5) as a measure of climate sensitivity and changes in CHAZ-based TC risk estimates (Supplementary Fig. 6 and Supplementary Fig. 7) and CHAZ frequency (Supplementary Fig. 8) and intensity changes (Supplementary Fig. 9). This presumably is due to the two hazard models' differing sensitivities of TC frequency, intensity, and/or other aspects of TC activity to warming. Since these responses of TCs to climate change are indeed uncertain (47) - with the response of TC frequency uncertain even in sign (52) - this uncertainty in our results may not be reducible given present science. In fact it is not obvious, given the small size of our multi-model ensemble, that the real uncertainty might not be even larger, i.e., that some possible TC hazard models might show changes with climate either larger or smaller than those in our ensemble.

Implications for interpretation of results, model development, and decision-making

We observed that socio-economic development is a more dominant risk driver than climate change in the STORM, CHAZ, and IBTrACS_p models, whereas the MIT model shows climate change as a comparably significant risk driver to socio-economic development (Fig. 2). This difference contributes to a narrower uncertainty distribution in TC risk change estimates derived from STORM, CHAZ, and IBTrACS_p, as opposed to those obtained from the MIT model (Fig. 3). These aspects also influence the sensitivity analysis. In a previous study, we interpreted the importance of the GCM choice for MIT-based TC risk change estimates as an indication of the relatively advanced state of modeling of TC hazard, and a consequence of the greater complexity of the MIT model, compared to the exposure and vulnerability models (28). However, our current findings suggest a different narrative, especially when comparing the MIT model with CHAZ. Despite CHAZ incorporating an additional hazard-related input factor (TCGI moisture variable; a detailed discussion of the role of TGCI for TC risk change estimates is provided in the Supplementary Information), its range of outputs is notably narrower than those from the MIT model. This shows that adding additional degrees of freedom need not necessarily lead to uncertainty increases. Instead, socio-economic development emerges as a more significant and uncertain risk driver in CHAZ-based results, indicating that uncertainty in TC risk assessments is not solely driven by model complexity. Rather, it also depends on how the uncertainty of hazard-related factors compares to that of exposure-related variables. We thus suggest that the relative magnitude of uncertainty associated with each input component of the risk model is also relevant for interpreting sensitivity analysis results.

While the mathematical concepts are straightforward—where *magnitude* often corresponds to the mode (peak) of probability density distributions and *uncertainty* affects the distribution's width (spread or variance) (13, 16, 46)—grasping their practical implications is important. For risk analysts and decision-makers, the balance between considering the full range of possible outcomes, including allegedly improbable tails, and focusing on the peaks of distributions hinges on their level of risk aversion and the stakes involved. Low risk aversion allows for prioritizing the most probable outcomes, streamlining decision-making towards the dominant risk drivers (*magnitude*), while uncertainties become secondary. In contrast, high-risk aversion necessitates a comprehensive analysis of all eventualities, in which case the significance of the central peak diminishes relative to *uncertainty*. This nuanced approach enables tailored risk management strategies that align with both the decision-maker's level of cautiousness and the specific context of the decision (53).

Classification of uncertainties and their implications

The outcomes of our uncertainty and sensitivity analyses reveal a strong dependency on the chosen risk model components, underscoring the necessity for careful interpretation and cautious extrapolation beyond the model boundaries. Our findings demonstrate not only that uncertainties vary with the TC model used but also that the relative sensitivities to different input factors shift as well. By mapping these outcomes to the aleatory, epistemic, and normative types of uncertainty - considering their quantifiability and potential for reduction- we aim to illustrate how these analyses can be extended to generate actionable insights that extend beyond the immediate model setup.

In our study, most input factors for uncertainty and sensitivity analysis represent forms of epistemic uncertainty. Scenario uncertainty is evident in varying hazard emission scenarios (*SSP hazard*), showing minor influence on the output uncertainty of TC risk change estimates across models. Conversely, scenario uncertainty of exposure, indicated by the SSP-based scaling factors for GDP growth (*SSP exposure*), is a key source of uncertainty in a wide range of outputs (Section 2.3). Model uncertainty in the hazard component is significant, particularly for hazard-related input factors like the GCM choice (*GCM*) and TCGI formulation (*TCGI moisture variable*). However, for the exposure component, model uncertainty related to the GDP model choice (*GDP model*) is small (19–21).

The reducibility of these uncertainties varies. Model uncertainty, particularly in the hazard component, is theoretically reducible through model refinement, enhanced data collection, and focused research (18, 21, 24, 54). In contrast, scenario uncertainty, which is inherently tied to future human choices, cannot be reduced in the same way. In the context of hazard modeling, scenario uncertainty may hold secondary importance due to its observed low sensitivity. However, exposure-related scenario uncertainty is high and thus becomes critically relevant from a decision-making standpoint. Although scenario uncertainty cannot be reduced, it can motivate decision-makers to favor scenarios of minimal risk. Specifically, the importance of scenario uncertainty in the exposure component (*SSP exposure*) may motivate decision-makers to choose policy options aligning with SSPs that induce the lowest TC risk increase.

Aleatory uncertainty is represented in the present study in the event subsampling of the hazard sets. Through sensitivity analysis, we observe divergent responses to subsampling (*Event subsampling base/future*) across different hazard models (Fig. 4, Supplementary Table 2). Specifically, the statistical-dynamical models MIT and CHAZ show no sensitivity to event subsampling, suggesting that they may inherently capture natural variability through their physics-based methodologies and the generation of new event sets for future climates. In contrast, the purely statistical models, IBTrACS_p and STORM, exhibited sensitivity to subsampling. This indicates that these models, which have the historical track sets at their foundation, may require the inclusion of a subsampling step to represent aleatory uncertainty adequately. Further validation is needed to strengthen this conclusion, however.

Despite its non-reducible nature (55), quantifying aleatory uncertainty is crucial, as demonstrated by the event subsampling in this study. Moreover, and perhaps counter-intuitively, while aleatory uncertainty is non-reducible (e.g., it is not even in principle possible to forecast the weather in 20 years due to the chaotic nature of the Earth system), it can be accurately represented in the form of a probability distribution. This differentiates it from epistemic uncertainty, which often is inherently indeterminate or not readily quantifiable. Accurately quantifying aleatory uncertainty thus helps differentiate it from epistemic uncertainty, guiding research efforts more effectively toward understanding and modeling the complex behaviors of natural systems.

Normative uncertainty is often interrelated with the other categories, but also extends beyond the focus of this paper into implications for how modelling results are used for societal decisions. Considering normative aspects in the context of scenario uncertainty in TC risk assessment, it is crucial to consider a wide range of scenarios to avoid blind spots in risk assessment. Unlike in policy-making, where particular scenarios or targets often represent a (normatively) favored developmental path (such as the Paris Agreement), excluding specific scenarios a priori in a risk setting could result in either under- or overestimation of risk. Furthermore, caution is also advised when considering whether to weight some scenarios as more likely than others, or to weight all scenarios equally, as improper weighting could exacerbate the risk of over- or underestimation.

Concerning normative facets in model uncertainty, the concept of "fitness for purpose" is vital (20). As a simple example, specifying risk only as EAD based on property values would tend to divert attention toward luxury coastal villas in Florida and away from informal coastal settlements in Bangladesh, even though TC impacts on the latter would have a much more negative effect on people's well-being. EAD would be an appropriate risk metric for estimating potential insurance payouts, whereas for humanitarian goals, risk metrics such as the number of people in poverty affected would be more appropriate for the modelling purpose. Hence different stakeholders and sectors require varied outputs from TC hazard models and different calculations of risk. Given practical constraints, selecting specific models early in the risk assessment process is often necessary, but this choice significantly influences the results. Indeed, as highlighted in our findings (Section 2.3), looking at the relative change or absolute impacts of TCs completely changes the narrative, not only in terms of the output values themselves (e.g., a few percent vs. several billion USD), but also in the sensitivity to input uncertainties (e.g., the dominance of hazard- or exposure- vs. impact function-related factors in Figures 4 vs. Supplementary Fig. 4). Hence, a bottom-up approach, incorporating stakeholder needs, goals and values to guide model selection, is recommended for tailoring risk assessments effectively (15).

Understanding the different types of uncertainties — aleatory, epistemic, and normative — is vital for risk modeling and informed decision-making. Linking these types of uncertainty to systematic uncertainty and sensitivity quantification across different TC hazard models, this study offers a nuanced view of TC risk assessment, which can guide future research and provide decision-critical insights. In particular, novel findings here are that the range of uncertainty in TC risk change is strongly model dependent, and further that which components of the modeling chain introduce the greatest sources of uncertainty also varies depending on choices in other components of that chain. This indicates that not only is the uncertainty itself uncertain, but so are which factors are most responsible for that uncertainty. Since our multi-model ensemble is small - with only four hazard models, for example - this raises the possibility that adding more models could change the conclusions quantitatively, or perhaps even qualitatively. We suspect that this situation is not unique to TCs, but may also apply to other aspects of climate risk. This suggests that humility in the use and interpretation of quantitative climate risk models is warranted, and that adaptation decisions should be based on multiple lines of evidence.

We also advocate for increased research on exposure and vulnerability modeling. While our uncertainty and sensitivity analysis might not explicitly highlight this need, we assert that this could be in part because these components are represented in a simple and reduced way in available datasets and the current modelling setup and fewer options are available to bracket the possibilities and define the uncertainties. The fact that exposure and vulnerability have been much less studied in forms that can readily be input into such modelling approaches (at least in the public domain) than the hazard offers immediate opportunities for impactful research, as these areas have a pronounced influence on results. In this study, exposure projections are based on uniform SSP-derived GDP growth factors. These were not designed to be used in a spatially explicit fashion (38) and fail to capture the spatial nuances of socio-economic development, such as urbanization patterns. For vulnerability, no viable options exist for simulating changes in future vulnerabilities at scale. Hence, achieving projections of exposures and vulnerabilities projections of exposures and vulnerabilities in spatially explicit forms that match the complexity of climate hazards demands an effort comparable to that of global climate modeling, encompassing both social development and adaptation strategies.

Providing reliable TC risk assessment, including uncertainty and sensitivity analysis, is important for emerging new fields like physical climate risk disclosure (3, 4) or changing traditional sectors like insurance. In both cases, rules by which climate risk science can be used appropriately to inform climate risk assessment have not yet been developed or are changing. As we move forward, it is essential to refine our models continually, choose models according to their application, and be critically aware of the normative assumptions that underlie our assessments. Ultimately, we aim to balance risk assessments that are both accurate and actionable.

4 Methods

4.1 Study regions

In this study, we assess future TC risk increases across four main regions, as shown in Figure 5 and established in Meiler et al. (2022) (15). These regions are chosen to broadly reflect distinct TC areas, focusing on the impact on land. Hence, we combine TCs originating in the North Atlantic and Eastern Pacific (AP) into one region to evaluate the socio-economic impact on national GDPs, accounting for countries with coastlines in multiple basins, such as the USA, Mexico, and Central American nations. Similarly, the Southern Hemisphere (SH) is treated as a unified region, with the North Indian Ocean (IO) and Western Pacific (WP) completing the geographical split.

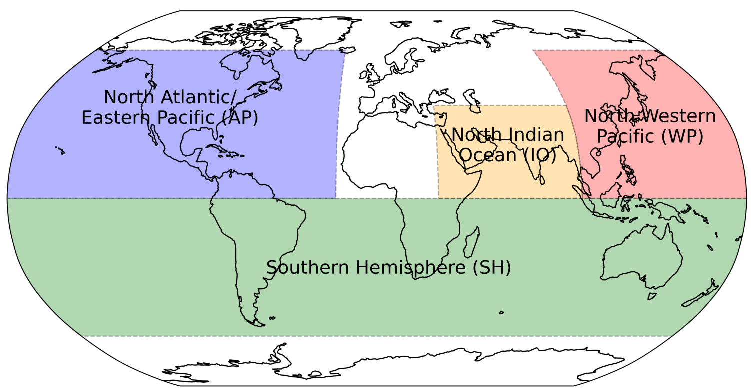

Fig. 5. Global study regions. North Atlantic/Eastern Pacific (AP, blue), North Indian Ocean (IO, orange), Southern Hemisphere (SH, green), Western Pacific (WP, red).

4.2 Tropical cyclone models

Different synthetic TC models exist, each with their unique modeling approach that influences the resulting TC event sets. Prominent methods commonly used for TC risk assessment are either purely statistical (34, 35) or coupled statistical-dynamical (30–33). Here, we briefly review the key similarities and differences of the global, academically-available TC models used in this study.

Statistical-dynamical TC models like the MIT (30, 31) and Columbia HAZard model (CHAZ) (32, 33) both use dynamical downscaling of TC tracks from reanalyses or climate model output. These models follow the three-step process of genesis, track, and intensity modelling. The main genesis mechanism of the MIT model is random seeding and natural selection (30, 31) while CHAZ uses a tropical cyclone genesis index (TCGI) (32, 33), which statistically links the occurrence of TCs to large-scale environmental conditions favorable for TC development. TC tracks are propagated via synthetic local winds from a beta-and-advection model (56) in both models. Intensity changes along the tracks are simulated using a dynamical model (MIT) (30, 31) or an autoregressive model using physics-based drivers (CHAZ) (32, 33).

In contrast, the fully statistical, global, open-source model STORM (34, 35) uses autoregressive formulas to simulate both the track and intensity of a TC. STORM run for present-day TC activity uses data from IBTrACS (37) and ECMWF's ERA-5 reanalysis (57) for input, generating synthetic TCs with characteristics consistent with observed statistics. For future climate simulations, Bloemendaal et al. (2022) (35) derived changes in key TC variables from four high-resolution GCM simulations (1979-2014 vs. 2015-2050) and applied these to TC variables from historical data. On this basis, they ran STORM to simulate future TC activity under climate change.

The fourth TC modelling approach featured in this study is the generation of probabilistic TC tracks from the IBTrACS records (37). This approach embedded in the CLIMADA platform (27) follows a simple interpolation method using a random-walk process (12, 36). The method was formulated to deduce a probabilistic track distribution from the historical observations, neglecting any particular physics, climate, or basin characteristics. A more detailed description can be found in the supplementary material of Gettelman et al. (2018) (12), and the handling of observations from the IBTrACS record (37) is detailed in Meiler et al. (2022) (15). Similarly to STORM, the probabilistic IBTrACS obtained from the CLIMADA platform can be climate-conditioned by changing their frequency and intensity according to scaling factors derived by Knutson et al. (2015) (58) for the CMIP5 generation of climate models. This approach is simpler than the future climate STORM modeling approach (35). Instead of rerunning a TC model based on several scaled key TC variables, it just applies scaling factors to hazard intensity and frequency. We note that, to date, climate-conditioned IBTrACS are not available for the newest generation of climate models (CMIP6). Furthermore, the resulting future TC event sets from the STORM model and probabilistic, climate-conditioned IBTrACS do not contain spatial variations compared to their present-day counterparts. In comparison, future MIT and CHAZ hazard sets are completely new event sets, including spatial variations of the tracks.

4.3 Tropical cyclone track sets

In this study, the MIT TC model (30, 31) was used to generate TC track sets from input of nine distinct GCMs (detailed in Supplementary Table 4) under three emission scenarios: SSP245, SSP370, and SSP585, which are part of the CMIP6 generation. The model simulations cover three timeframes: the present-day reference period (1995-2014), a mid-century period (2041-2060), and a late-century period (2081-2100). The model generated 500 TCs each year within these periods using the three-step process of genesis, track, and intensity modelling described in the previous section. The annual variation in the number of TCs is influenced by the specific boundary conditions set by the GCMs, such as potential intensity and wind shear, affecting how many of the initial seeds develop into full TCs. The final yearly TC frequency is determined by comparing the initial seed count to the calibrated total of 500 events per year.

CHAZ (32, 33) was used to generate TC event sets for three emission scenarios (SSP245, SSP370, SSP585) drawing from six (CESM2, CNRM-CM6-1, EC-Earth3, IPSL-CM6A-LR, MIROC6, UKESM1-0-LL) of the nine CMIP6 GCMs also utilized by the MIT model (cf. Supplementary Table 4) and two distinctly different choices of moisture variable used in the TCGI component of CHAZ (33). CHAZ is downscaled for every combination of emission scenario, GCM, and TCGI with 10 different realizations of the genesis model and resulting tracks. For each genesis realization, 40 ensembles of the intensity model are produced. In this study, we use all 10 genesis ensembles but select only 8 out of the 40 intensity ensembles. This results in 80 ensemble members, reducing computational costs while maintaining a crucial sample size.

Analogous to the MIT hazard sets, we contrast TC event sets for a present climate reference state (1995-2014) with two future periods: mid-century (2041-2060) and end of the century (2081-2100). Additionally, CHAZ hazard sets require a frequency bias correction (15, 32, 59). We adjust the hazard frequency of all reference state hazard sets using the observed frequencies in each basin. Numbers for the observed IBTrACS genesis events are derived from Bloemendaal et al. (2020; Table 3) (34) and are combined to values relevant to the study regions of this manuscript (Fig. 5). Each TC in the baseline hazard set is adjusted to ensure the overall frequency aligns with the observed average. This adjusted frequency is then applied to the TCs in the future climate hazard sets. While each future TC maintains the same frequency as a present-day counterpart, the entire event set's frequency shifts due to variations in the total storm count, thereby reflecting the hazard set's frequency changes in the future.

TC track sets from the statistical model STORM were used as released by Bloemendaal et al. (2020, 2022) (34, 35) representing 10 000 years of present-day (1980-2018) (34) and future (SSP585; 2015–2050) synthetic TCs from an ensemble of four high-resolution climate models. Note that future STORM TC tracks are only available for a single emission scenario (SSP585) and the middle-of-the-century time period.

Finally, using the random walk algorithm of the CLIMADA platform as described in the previous section, we generated a set of 24 probabilistic tracks for each observed TC between 1990 and 2010 for this study. Upon generating wind fields from these tracks (cf. Section 4.5) using two different parametric wind models (60, 61), the hazard sets are climate-conditioned by applying constant, basin-specific factors to the tracks' intensity and frequency. These factors were derived from the meta-analysis by Knutson et al. (2015) (58) summarizing the effects of climate change on TCs by CMIP5 climate models under RCP4.5 projections for the late 21st century. A linear scaling approach is used to estimate parameters for different future periods and the other three RCP scenarios (2.6, 6.0, 8.5) according to the RCP database (62). Note that we did not generate climate-conditioned hazard sets for the RCP8.5 scenario at the end of the century as the current implementation of the respective module on the

CLIMADA platform produces erroneous negative frequencies. In the remainder of this study, we refer to hazard sets generated via this approach as *IBTrACS_p*.

4.4 Risk model CLIMADA

The open-source, probabilistic climate risk model CLIMADA integrates climate and weather-related hazards with the exposure and vulnerability of assets, populations, and infrastructure on a global scale (27). Developed as a community initiative, its Python 3 source code is freely accessible under the GNU General Public License Version 3. In this study, we utilize CLIMADA v3.2 (63) to evaluate the projected increase in direct economic losses from TCs in the mid and late 21st century, relative to a contemporary baseline. Damage estimates are calculated at a spatial resolution of 300 arc seconds (approximately 10 km at the equator).

4.5 Tropical cyclone hazard

In CLIMADA, the TC hazard is represented by a two-dimensional wind field, created by integrating TC track sets with a parametric wind model. This study employs two distinct wind models, based on the parameterizations from Holland (2008) (60) and Emanuel and Rotunno (2011) (61), applied to all TC track sets described in Section 4.3. These wind models calculate the gridded 1-minute sustained winds at 10 meters above ground, comprising both a circular wind field component and the translational wind speed generated by the TC's movement. A key difference between the models lies in how they compute the (absolute) angular velocity from the wind profile. In both models, an attenuation factor, as suggested by Geiger et al. (2018) (9), is used to model the reduction of the translational wind component with distance from the cyclone center. For this study, wind fields are computed at a resolution of 300 arc seconds. CLIMADA utilizes the peak lifetime wind speed at each location as the hazard variable, disregarding values below 34 knots (17.5 meters per second).

4.6 Asset exposure representations

We generated a spatially explicit, gridded dataset of asset exposure values using the LitPop method. This approach disaggregates national asset value totals to grid cells based on a combination of nightlight intensity (Lit) and population density (Pop), as proposed by Eberenz et al. (2020) (64). The reference exposure layer for the present day is computed at a resolution of 300 arc seconds, using the Gross Domestic Product (GDP) values (in USD) from 2005; approximately centered in the present-day TC track set periods. For future exposure representations - identical to Meiler et al. (2023a, 2023b) (28, 29) - we use economic growth factors from the SSPs to approximate socio-economic development, drawing from the SSP database that documents quantitative projections of SSPs and related scenarios (38). SSPs outline five potential trajectories for global changes in population, economic growth, technology, governance, and social norms over the next century, with a focus here on GDP projections as a measure of economic development. Three alternative GDP interpretations by the Organization for Economic Co-operation and Development (OECD) (39), the International Institute for Applied Systems Analysis (IIASA) (40), and the Potsdam Institute for Climate Impact Research (PIK) (41) are considered, which, despite being based on the same SSP assumptions for economic growth determinants, vary in methods and results. We specifically query GDP growth factors for 2050 and 2090 for each country across all five SSPs from these models, scaling the reference asset values accordingly for the two future time periods across all scenarios. In this approach, the spatial distribution of assets remains static, not accounting for potential spatial shifts in socio-economic factors.

4.7 Impact functions

In risk assessment, impact functions represent vulnerability, describing how hazard intensity translates to damage on assets. In this study, we employ regionally calibrated impact functions as developed by Eberenz et al. (2021) (42). These functions are fitted to nine different global regions, reflecting the diverse vulnerability levels across the world. For this study, we applied the same impact functions to all four synthetic TC track sets. In contrast to the well-developed methodologies for exposure and particularly hazard modeling, no viable options exist for simulating changes in future vulnerabilities. Therefore, we do not hypothesize about changes to the vulnerability function in the future but test uncertainties by varying the vulnerability function's slope parameter of regionally-calibrated vulnerability functions (42) across a wide range.

4.8 Uncertainty and sensitivity analysis

For this study's uncertainty and sensitivity quantification, we use the *unsequa* module on the CLIMADA platform (13). We extended the unsequa module to compute uncertainties for changes in risk directly. These functionalities are now also publically available as 'CalcDeltaImpact' in CLIMADA v.4.1.1 or higher. The module seamlessly integrates the *SALib* Python package (65) and allows for uncertainty and sensitivity analyses of all CLIMADA-based risk calculations. A central aspect of uncertainty and sensitivity analysis is determining input factors and characterizing their variability space (13, 16, 66). This section delineates our approach to address uncertainties in inputs related to (future) TC hazards, exposure, and vulnerability within the context of our study (Figure 1).

We choose from a discrete list of scientifically justified alternative versions of future climate and socio-economic systems. We prioritize this approach over defining additive or multiplicative perturbations for each input factor because it avoids the challenges of defining perturbations without relevant information, directly relates the output to chosen input combinations, and circumvents assumptions about the likelihood of specific input scenarios. Specifically, we define five input factors characterizing the hazard components, three for the exposure and one for the impact function (see Table 1). For event subsampling, targeting the aleatory uncertainty of the hazard set, we favor continuous sampling to better represent its inherent variability. Continuous sampling is also employed for the parameters describing the impact function due to the absence of a scientifically supported discrete alternative.

Table 1. Input factors and their variability space. The first column lists all input factors of the uncertainty and sensitivity analysis, indicating which risk model component they relate to. Variable names, as referred to in the text and figures of this study, are listed in the second column; short names thereof in the third; the type of the parameter range in the fourth; and the actual parameter ranges for each hazard model in the last four columns.

Input factor	Variable name	Short name	Type	Range			
				MIT	STORM	CHAZ	IBTrACS_p[a]
Hazard: GCM	GCM	gc_model	discrete	1 - 9	1 - 4	1 - 6	N/A
Hazard: Emission scenario	SSP hazard	ssp_haz	discrete	1 - 3	N/A	1 - 3	1 - 4 (3 for 2100)
Hazard: Wind Model	Wind model	wind_model	discrete	1 - 2	1 - 2	1 - 2	1 - 2
Hazard: Moisture variable TCGI	Moisture variable TCGI	tcgi_var	discrete	N/A	N/A	1 - 2	N/A
Hazard: Bootstrapping	Event subsampling base/future	HE_base/HE_fut	continuous	80 % of every year	1/10 ensembles	80 % of event set	80 % of event set
Exposure: SSP-based GDP scaling	SSP exposure	ssp_exp	discrete	1 - 5			
Exposure: GDP model	GDP model	gdp_model	discrete	1 - 3			
Exposure: m,n scaling LitPop	Exposure urban/rural weighting	mn_scaling	discrete	1 - 9			
Impact functions	Vulnerability function midpoint	v_half	continuous	within IQR of regional TC calibration[b]			

[a] CMIP5

[a] Eberenz et al. (2021) (42)

We then generate a set of N=2^{10} (equal to 1024) samples of the input parameters across the four distinct model setups for each TC model. We note that the sample size is large enough for the uncertainty analysis to converge. This means that the analysis has reached a state where additional samples do not significantly change the results. The Sobol' sampling algorithm (44, 45) is applied to the resulting approximately 20 000 input factor combinations. For each sample, we calculate the TC risk change, resulting in distributions for both analyzed risk metrics (change in EAD and 100-yr event). This output distribution underpins the uncertainty analysis and initiates the sensitivity analysis. Utilizing the Sobol' quasi-Monte Carlo sequence (44), we present first- and total-order sensitivity indices to estimate each input factor's contribution to output variance. Specifically, the first-order sensitivity index measures the direct impact of a single input factor on the output uncertainty, independent of other factors. The total-order sensitivity index, on the other hand, captures both the direct effects and any potential interactions with other input parameters. Together, these indices provide a comprehensive view of how changes in input variables influence the uncertainty in our results.

References

1. Keenan, J. M. A climate intelligence arms race in financial markets. *Science* **365**, 1240–1243, DOI: 10.1126/science.aay8442 (2019).
2. Condon, M. Climate Services: The Business of Physical Risk, DOI: 10.2139/ssrn.4396826 (2023).
3. Arribas, A. *et al.* Climate risk assessment needs urgent improvement. *Nat. Commun.* **13**, 4326, DOI: 10.1038/s41467-022-31979-w (2022).
4. Fiedler, T. *et al.* Business risk and the emergence of climate analytics. *Nat. Clim. Chang.* **11**, 87–94, DOI: 10.1038/s41558-020-00984-6 (2021).
5. Braman, L. M., Suarez, P. & Aalst, M. K. v. Climate change adaptation: integrating climate science into humanitarian work. *Int. Rev. Red Cross* **92**, 693–712, DOI: 10.1017/S1816383110000561 (2010).
6. Jones, L. *et al.* Ensuring climate information guides long-term development. *Nat. Clim. Chang.* **5**, 812–814, DOI: 10.1038/nclimate2701 (2015).
7. Coughlan de Perez, E. & Mason, S. J. Climate information for humanitarian agencies: some basic principles. *Earth Perspectives* **1**, 11, DOI: 10.1186/2194-6434-1-11 (2014).
8. Enenkel, M. & Kruczkiewicz, A. The Humanitarian Sector Needs Clear Job Profiles for Climate Science Translators Now More than Ever. *Bull. Am. Meteorol. Soc.* **103**, E1088–E1097, DOI: 10.1175/BAMS-D-20-0263.1 (2022).
9. Geiger, T., Frieler, K. & Bresch, D. N. A global historical data set of tropical cyclone exposure (TCE-DAT). *Earth Syst. Sci. Data* **10**, 185–194, DOI: 10.5194/essd-10-185-2018 (2018).

10. Berlemann, M. & Wenzel, D. Hurricanes, economic growth and transmission channels: Empirical evidence for countries on differing levels of development. *World Dev.* **105**, 231–247, DOI: 10.1016/j.worlddev.2017.12.020 (2018).

11. Mendelsohn, R., Emanuel, K., Chonabayashi, S. & Bakkensen, L. The impact of climate change on global tropical cyclone damage. *Nat. Clim. Chang.* **2**, 205–209, DOI: 10.1038/nclimate1357 (2012).

12. Gettelman, A., Bresch, D. N., Chen, C. C., Truesdale, J. E. & Bacmeister, J. T. Projections of future tropical cyclone damage with a high-resolution global climate model. *Clim. Chang.* **146**, 575–585, DOI: 10.1007/s10584-017-1902-7 (2018).

13. Kropf, C. M. *et al.* Uncertainty and sensitivity analysis for probabilistic weather and climate-risk modelling: an implementation in CLIMADA v.3.1.0. *Geosci. Model. Dev.* **15**, 7177–7201, DOI: 10.5194/gmd-15-7177-2022 (2022).

14. IPCC. *Managing the Risks of Extreme Events and Disasters to Advance Climate Change Adaptation. A Special Report of Working Groups I and II of the Intergovernmental Panel on Climate Change [Field, C.B., V. Barros, T.F. Stocker, D. Qin, D.J. Dokken, K.L. Ebi, M.D* (2012). Publication Title: Research Report ISSN: 0009-4978.

15. Meiler, S. *et al.* Intercomparison of regional loss estimates from global synthetic tropical cyclone models. *Nat. Commun.* **13**, 6156, DOI: 10.1038/s41467-022-33918-1 (2022).

16. Pianosi, F. *et al.* Sensitivity analysis of environmental models: A systematic review with practical workflow. *Environ. Model. & Softw.* **79**, 214–232, DOI: 10.1016/j.envsoft.2016.02.008 (2016).

17. Wagener, T., Reinecke, R. & Pianosi, F. On the evaluation of climate change impact models. *WIREs Clim. Chang.* e772, DOI: 10.1002/wcc.772 (2022).

18. Walker, W. *et al.* Defining Uncertainty: A Conceptual Basis for Uncertainty Management in Model-Based Decision Support. *Integr. Assess.* **4**, 5–17, DOI: 10.1076/iaij.4.1.5.16466 (2003).

19. Hawkins, E. & Sutton, R. The Potential to Narrow Uncertainty in Regional Climate Predictions. *Bull. Am. Meteorol. Soc.* **90**, 1095–1108, DOI: 10.1175/2009BAMS2607.1 (2009).

20. Parker, W. S. Predicting weather and climate: Uncertainty, ensembles and probability. *Stud. Hist. Philos. Sci. Part B: Stud. Hist. Philos. Mod. Phys.* **41**, 263–272, DOI: 10.1016/j.shpsb.2010.07.006 (2010).

21. Knutti, R. Climate Model Confirmation: From Philosophy to Predicting Climate in the Real World. In A. Lloyd, E. & Winsberg, E. (eds.) *Climate Modelling: Philosophical and Conceptual Issues*, 325–359, DOI: 10.1007/978-3-319-65058-6_11 (Springer International Publishing, Cham, 2018).

22. Moss, R. H. *et al.* The next generation of scenarios for climate change research and assessment. *Nature* **463**, 747–756, DOI: 10.1038/nature08823 (2010).

23. Bradley, R. & Drechsler, M. Types of Uncertainty. *Erkenntnis* **79**, 1225–1248, DOI: 10.1007/s10670-013-9518-4 (2014). : Springer Verlag.

24. Bradley, R. & Steele, K. Making Climate Decisions. *Philos. Compass* **10**, 799–810, DOI: 10.1111/phc3.12259 (2015). _eprint: https://onlinelibrary.wiley.com/doi/pdf/10.1111/phc3.12259.

25. Mayer, L. *et al.* Understanding Scientists' Computational Modeling Decisions About Climate Risk Management Strategies Using Values-Informed Mental Models. *Glob. Environ. Chang.* **42**, 107–116, DOI: 10.1016/j.gloenvcha.2016.12.007 (2017).

26. Hansson, S. O. Evaluating the Uncertainties. In Hansson, S. O. & Hirsch Hadorn, G. (eds.) *The Argumentative Turn in Policy Analysis: Reasoning about Uncertainty*, Logic, Argumentation & Reasoning, 79–104, DOI: 10.1007/978-3-319-30549-3_4 (Springer International Publishing, Cham, 2016).

27. Aznar-Siguan, G. & Bresch, D. N. CLIMADA v1: A global weather and climate risk assessment platform. *Geosci. Model. Dev.* **12**, 3085–3097, DOI: 10.5194/gmd-12-3085-2019 (2019).

28. Meiler, S., Ciullo, A., Kropf, C. M., Emanuel, K. & Bresch, D. N. Uncertainties and sensitivities in the quantification of future tropical cyclone risk. *Commun. Earth & Environ.* **4**, 1–10, DOI: 10.1038/s43247-023-00998-w (2023).

29. Meiler, S., Ciullo, A., Bresch, D. N. & Kropf, C. M. Uncertainty and sensitivity analysis for probabilistic, global modelling of future tropical cyclone risk. 8, DOI: https://doi.org/10.25546/103244 (Dublin, Ireland, 2023).

30. Emanuel, K., Ravela, S., Vivant, E. & Risi, C. A Statistical Deterministic Approach to Hurricane Risk Assessment. *Bull. Am. Meteorol. Soc.* **87**, S1–S5, DOI: 10.1175/bams-87-3-emanuel (2006).

31. Emanuel, K. A. The Hurricane - Climate Connection. *Bull. Am. Meteorol. Soc.* **89**, ES10–ES20, DOI: 10.1175/BAMS-89-5-Emanuel (2008).

32. Lee, C. Y., Tippett, M. K., Sobel, A. H. & Camargo, S. J. An environmentally forced tropical cyclone hazard model. *J. Adv. Model. Earth Syst.* **10**, 223–241, DOI: 10.1002/2017MS001186 (2018).

33. Lee, C. Y., Camargo, S. J., Sobel, A. H. & Tippett, M. K. Statistical–Dynamical Downscaling Projections of Tropical Cyclone Activity in a Warming Climate: Two Diverging Genesis Scenarios. *J. Clim.* **33**, 4815–4834, DOI: 10.1175/jcli-d-19-0452.1 (2020).

34. Bloemendaal, N. *et al.* Generation of a global synthetic tropical cyclone hazard dataset using STORM. *Sci. Data* **7**, 40,

DOI: 10.1038/s41597-020-0381-2 (2020).
35. Bloemendaal, N. *et al.* A globally consistent local-scale assessment of future tropical cyclone risk. *Sci. Adv.* **8**, eabm8438, DOI: 10.1126/sciadv.abm8438 (2022).
36. Kleppek, S. *et al.* Tropical cyclones in ERA-40: A detection and tracking method. *Geophys. Res. Lett.* **35**, DOI: 10.1029/2008GL033880 (2008).
37. Knapp, K. R., Kruk, M. C., Levinson, D. H., Diamond, H. J. & Neumann, C. J. The International Best Track Archive for Climate Stewardship (IBTrACS). *Bull. Am. Meteorol. Soc.* **91**, 363–376, DOI: 10.1175/2009BAMS2755.1 (2010).
38. Riahi, K. *et al.* The Shared Socioeconomic Pathways and their energy, land use, and greenhouse gas emissions implications: An overview. *Glob. Environ. Chang.* **42**, 153–168, DOI: 10.1016/j.gloenvcha.2016.05.009 (2017).
39. Dellink, R., Chateau, J., Lanzi, E. & Magné, B. Long-term economic growth projections in the Shared Socioeconomic Pathways. *Glob. Environ. Chang.* **42**, 200–214, DOI: 10.1016/j.gloenvcha.2015.06.004 (2017).
40. Crespo Cuaresma, J. Income projections for climate change research: A framework based on human capital dynamics. *Glob. Environ. Chang.* **42**, 226–236, DOI: 10.1016/j.gloenvcha.2015.02.012 (2017).
41. Leimbach, M., Kriegler, E., Roming, N. & Schwanitz, J. Future growth patterns of world regions – A GDP scenario approach. *Glob. Environ. Chang.* **42**, 215–225, DOI: 10.1016/j.gloenvcha.2015.02.005 (2017).
42. Eberenz, S., Lüthi, S. & Bresch, D. N. Regional tropical cyclone impact functions for globally consistent risk assessments. *Nat. Hazards Earth Syst. Sci.* **21**, 393–415, DOI: 10.5194/nhess-21-393-2021 (2021).
43. Lemieux, C. *Monte Carlo and Quasi-Monte Carlo Sampling* (Springer Science & Business Media, 2009).
44. Sobol, I. M. Global sensitivity indices for nonlinear mathematical models and their Monte Carlo estimates. *Math. Comput. Simul.* DOI: 10.1016/S0378-4754(00)00270-6 (2001).
45. Saltelli, A. *et al.* Variance based sensitivity analysis of model output. Design and estimator for the total sensitivity index. *Comput. Phys. Commun.* **181**, 259–270, DOI: 10.1016/j.cpc.2009.09.018 (2010).
46. Saltelli, A. *et al. Global Sensitivity Analysis: The Primer* (John Wiley & Sons, Ltd, 2008).
47. Knutson, T. *et al.* Tropical cyclones and climate change assessment part II: Projected response to anthropogenic warming. *Bull. Am. Meteorol. Soc.* **101**, E303–E322, DOI: 10.1175/BAMS-D-18-0194.1 (2020).
48. Emanuel, K. Environmental Factors Affecting Tropical Cyclone Power Dissipation. *J. Clim.* **20**, 5497–5509, DOI: 10.1175/2007JCLI1571.1 (2007).
49. Emanuel, K. A. & Nolan, D. S. Tropical cyclone activity and global climate (2004). Publication Title: Preprints, 26th Conf. on Hurricanes and Tropical Meteorology, Miami, FL, Amer. Meteor. Soc., 240–241.
50. Emanuel, K. Tropical cyclone activity downscaled from NOAA-CIRES Reanalysis, 1908–1958. *J. Adv. Model. Earth Syst.* **2**, 1, DOI: 10.3894/JAMES.2010.2.1 (2010).
51. Rappin, E. D., Nolan, D. S. & Emanuel, K. A. Thermodynamic control of tropical cyclogenesis in environments of radiative-convective equilibrium with shear: Tropical Cyclogenesis in Variable Climates. *Q. J. Royal Meteorol. Soc.* **136**, 1954–1971, DOI: 10.1002/qj.706 (2010).
52. Sobel, A. H. *et al.* Tropical cyclone frequency. *Earth's Futur.* e2021EF002275, DOI: 10.1029/2021EF002275 (2021). Publisher: John Wiley & Sons, Ltd ISBN: 10.1029/2021.
53. Roussos, J., Bradley, R. & Frigg, R. Making Confident Decisions with Model Ensembles. *Philos. Sci.* **88**, 439–460, DOI: 10.1086/712818 (2021).
54. Curry, J. A. & Webster, P. J. Climate Science and the Uncertainty Monster. *Bull. Am. Meteorol. Soc.* **92**, 1667–1682, DOI: 10.1175/2011BAMS3139.1 (2011). : American Meteorological Society Section: Bulletin of the American Meteorological Society.
55. Henrion, M. & Morgan, M. G. The Nature and Sources of Uncertainty. In *Uncertainty: A Guide to Dealing with Uncertainty in Quantitative Risk and Policy Analysis*, 47–72, DOI: 10.1017/CBO9780511840609.005 (Cambridge University Press, Cambridge, 1990).
56. Marks, D. G. The Beta and advection model for hurricane track forecasting (1992).
57. Hersbach, H. *et al.* Global reanalysis: goodbye ERA-Interim, hello ERA5. *ECMWF Newsl.* 17–24, DOI: 10.21957/vf291hehd7 (2019).
58. Knutson, T. R. *et al.* Global projections of intense tropical cyclone activity for the late twenty-first century from dynamical downscaling of CMIP5/RCP4.5 scenarios. *J. Clim.* **28**, 7203–7224, DOI: 10.1175/JCLI-D-15-0129.1 (2015).
59. Sobel, A. H. *et al.* Tropical cyclone hazard to mumbai in the recent historical climate. *Mon. Weather. Rev.* **147**, 2355–2366, DOI: 10.1175/MWR-D-18-0419.1 (2019).
60. Holland, G. A revised hurricane pressure-wind model. *Mon. Weather. Rev.* **136**, 3432–3445, DOI: 10.1175/2008MWR2395.1 (2008).
61. Emanuel, K. & Rotunno, R. Self-stratification of tropical cyclone outflow. Part I: Implications for storm structure. *J. Atmospheric Sci.* **68**, 2236–2249, DOI: 10.1175/JAS-D-10-05024.1 (2011).

62. IIASA. RCP Database (Version 2.0.5) (2009).
63. gabrielaznar *et al.* CLIMADA-project/climada_python: v3.2.0, DOI: 10.5281/zenodo.6807463 (2022).
64. Eberenz, S., Stocker, D., Röösli, T. & Bresch, D. N. Asset exposure data for global physical risk assessment. *Earth Syst. Sci. Data* **12**, 817–833, DOI: 10.5194/essd-12-817-2020 (2020).
65. Herman, J. & Usher, W. SALib: An open-source Python library for Sensitivity Analysis. *J. Open Source Softw.* **2**, 97, DOI: 10.21105/joss.00097 (2017).
66. Saltelli, A. *et al.* Why so many published sensitivity analyses are false: A systematic review of sensitivity analysis practices. *Environ. Model. Softw.* **114**, 29–39, DOI: 10.1016/j.envsoft.2019.01.012 (2019).
67. Bloemendaal, N. *et al.* STORM IBTrACS present climate synthetic tropical cyclone tracks, DOI: 10.4121/UUID:82C1DC0D-5485-43D8-901A-CE7F26CDA35D (2020).
68. Bloemendaal, N. *et al.* STORM Climate Change synthetic tropical cyclone tracks, DOI: 10.4121/14237678.V2 (2023).
69. Aznar-Siguan, G. *et al.* CLIMADA-project/climada_python: v4.0.1, DOI: 10.5281/zenodo.8383171 (2023).
70. Meiler, S. simonameiler/TC_future_risk_uncertainty_multi-model, DOI: 10.5281/zenodo.10715404 (2024).
71. Emanuel, K. Response of Global Tropical Cyclone Activity to Increasing CO2: Results from Downscaling CMIP6 Models. *J. Clim.* **34**, 57–70, DOI: 10.1175/JCLI-D-20-0367.1 (2021).
72. Danabasoglu, G. *et al.* The Community Earth System Model Version 2 (CESM2). *J. Adv. Model. Earth Syst.* **12**, e2019MS001916, DOI: 10.1029/2019MS001916 (2020). _eprint: https://onlinelibrary.wiley.com/doi/pdf/10.1029/2019MS001916.
73. Voldoire, A. *et al.* Evaluation of CMIP6 DECK Experiments With CNRM-CM6-1. *J. Adv. Model. Earth Syst.* **11**, 2177–2213, DOI: 10.1029/2019MS001683 (2019).
74. EC Earth Consortium. EC-Earth-Consortium EC-Earth3 model output prepared for CMIP6 ScenarioMIP ssp245, DOI: 10.22033/ESGF/CMIP6.4880 (2019).
75. Li, L. CAS FGOALS-g3 model output prepared for CMIP6 ScenarioMIP ssp245, DOI: 10.22033/ESGF/CMIP6.3469 (2019).
76. Hourdin, F. *et al.* LMDZ6A: The Atmospheric Component of the IPSL Climate Model With Improved and Better Tuned Physics. *J. Adv. Model. Earth Syst.* **12**, e2019MS001892, DOI: 10.1029/2019MS001892 (2020). _eprint: https://onlinelibrary.wiley.com/doi/pdf/10.1029/2019MS001892.
77. Tatebe, H. *et al.* Description and basic evaluation of simulated mean state, internal variability, and climate sensitivity in MIROC6. *Geosci. Model. Dev.* **12**, 2727–2765, DOI: 10.5194/gmd-12-2727-2019 (2019).
78. Müller, W. A. *et al.* A Higher-resolution Version of the Max Planck Institute Earth System Model (MPI-ESM1.2-HR). *J. Adv. Model. Earth Syst.* **10**, 1383–1413, DOI: 10.1029/2017MS001217 (2018).
79. Yukimoto, S. *et al.* MRI MRI-ESM2.0 model output prepared for CMIP6 ScenarioMIP ssp245, DOI: 10.22033/ESGF/CMIP6.6910 (2019).
80. Sellar, A. A. *et al.* Implementation of U.K. Earth System Models for CMIP6. *J. Adv. Model. Earth Syst.* **12**, e2019MS001946, DOI: 10.1029/2019MS001946 (2020).
81. Hausfather, Z., Marvel, K., Schmidt, G. A., Nielsen-Gammon, J. W. & Zelinka, M. Climate simulations: recognize the 'hot model' problem. *Nature* **605**, 26–29, DOI: 10.1038/d41586-022-01192-2 (2022).
82. Tippett, M. K., Camargo, S. J. & Sobel, A. H. A poisson regression index for tropical cyclone genesis and the role of large-scale vorticity in genesis. *J. Clim.* **24**, 2335–2357, DOI: 10.1175/2010JCLI3811.1 (2011).
83. Camargo, S. J., Tippett, M. K., Sobel, A. H., Vecchi, G. A. & Zhao, M. Testing the performance of tropical cyclone genesis indices in future climates using the HiRAM model. *J. Clim.* **27**, 9171–9196, DOI: 10.1175/JCLI-D-13-00505.1 (2014).

Acknowledgements

Funding

CMK acknowledges funding from the European Union's Horizon 2020 research and innovation program under grant agreement No 820712 (PROVIDE).
AHS, CYL, SJC acknowledge support from the Swiss Re Foundation (SREF 6437).
KE's contribution is part of the MIT Climate Grand Challenge on Weather and Climate Extremes and has received support through the generosity of Eric and Wendy Schmidt by recommendation of Schmidt Futures as part of its Virtual Earth System Research Institute (VESRI).

Author contributions statement

Conceptualization: SM
Methodology: SM, CMK

Investigation: SM
Visualization: SM, CMK
Datasets: CYL, SJC, AHS, NB, KE
Supervision: CMK, KE, DNB
Writing — original draft: SM
Writing — review & editing: SM, CMK, JWM, CYL, SJC, AHS, NB, KE, DNB

Competing interests

AHS is a member of the Board of Advisors of Jupiter Intelligence, Inc.
KE is on the advisory board of First Street Foundation and the Chief Scientific Officer of WindRiskTech, LLC.
DNB is co-founder and chairman of CLIMADA Technologies Ltd.
All other authors (SM, CMK, JWM, CYL, SJC) declare no competing interests.

Data Availability

The synthetic TC data from the MIT model are property of WindRiskTech L.L.C., which is a company that provides hurricane risk assessments to clients worldwide. Upon request (info@windrisktech.com), the company provides datasets free of charge to scientific researchers, subject to a non-redistribution agreement. CHAZ is an open-source model and can be downloaded at (`https://github.com/cl3225/CHAZ`). The CHAZ data are available to scientific reseachers upon request to the CHAZ development team at Columbia University. The statistical model STORM is fully open: the model code can be obtained from GitHub (`https://github.com/NBloemendaal`) under the terms of the GNU General Public License Version 3 and datasets are available from the 4TU.ResearchData data repository (67, 68), licensed as public domain (CC0). The IBTrACS_p TCs are obtained from the random-walk process directly executed in CLIMADA (12, 27, 36). All of the TC track sets can be fed into CLIMADA to calculate TC impacts, independent from their respective licenses. For this study we used the Python (3.9+) version of CLIMADA release v4.1.1 (69). Source code is openly and freely available under the terms of the GNU General Public License Version 3 (27).

Code Availability

Code to reproduce the results of this paper is available at a GitHub repository with the identifier https://10.5281/zenodo.10715404 (70).

Supplementary Information for article "Navigating uncertainty and sensitivity analysis of future tropical cyclone risk estimates"

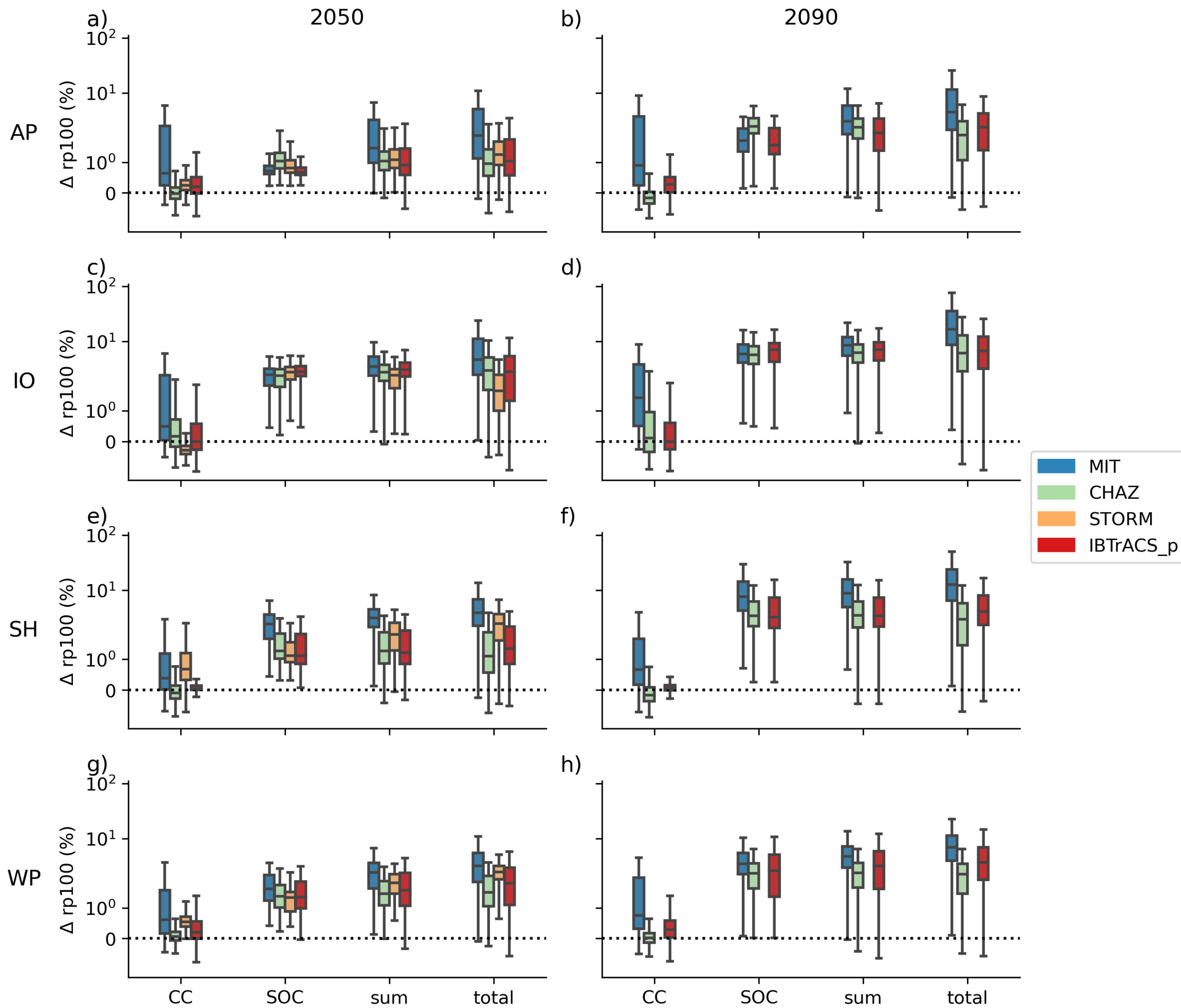

Supplementary Fig. 1. Drivers of future tropical cyclone risk change. Relative change in 100-yr event (rp100) by 2050 (left panels) and 2090 (right panels) due to climate change (CC), socio-economic development (SOC), the product of CC and SOC calculated from the sum of their log values (sum) and both drivers interacting (total) with respect to the historical baseline. The relative change 100-yr event is reported for the four study regions (North Atlantic/Eastern Pacific (AP), North Indian Ocean (IO), Southern Hemisphere (SH), and North Western Pacific (WP)). Boxplots are shown for the four models MIT (blue), CHAZ (green), STORM (orange), IBTrACS_p (red) and display the interquartile range (IQR) for the uncertainty over all input factors (see Methods), while the whiskers extend to 1.5 times the IQR. More extreme points (outliers) are not shown. Note that STORM results are only available for 2050.

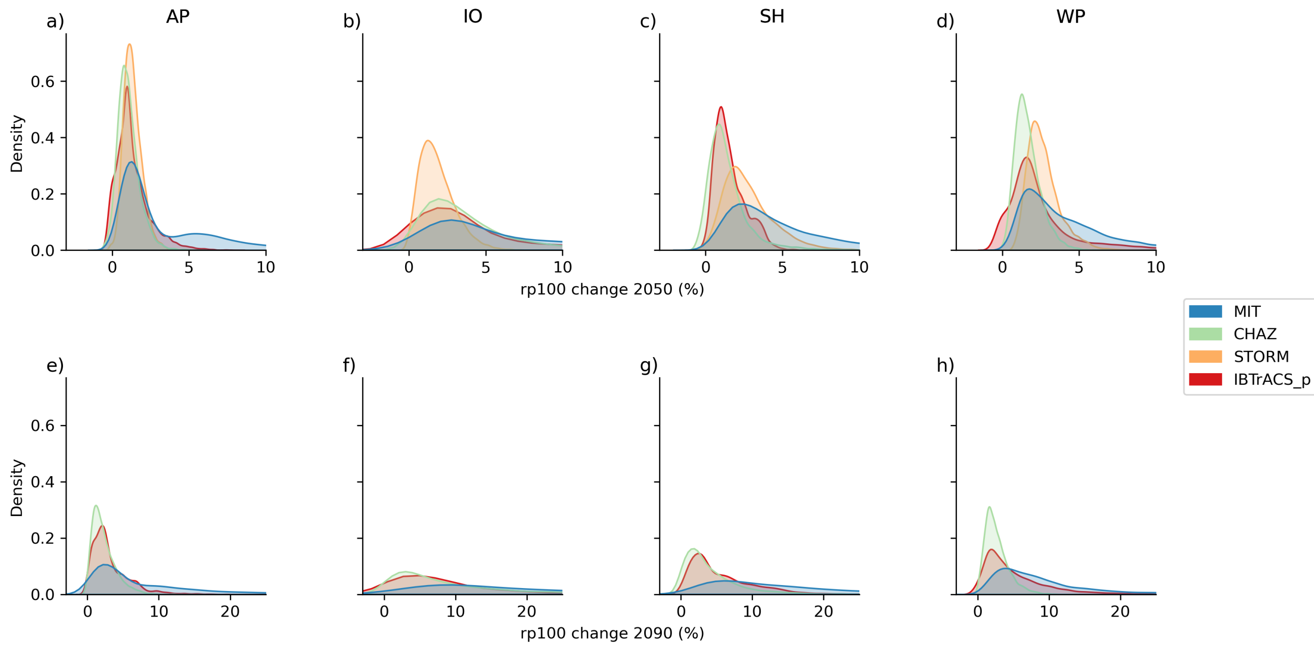

Supplementary Fig. 2. Uncertainty distribution of TC risk change. Kernel density estimation plots showcasing the uncertainty distribution of estimated relative change in 100-yr event (rp100) across study regions (North Atlantic/Eastern Pacific (AP), North Indian Ocean (IO), Southern Hemisphere (SH), and North Western Pacific (WP)) for the years 2050 and 2090. Each subplot represents a specific region and year combination, with different models (MIT, CHAZ, STORM, IBTrACS_p) depicted in distinct colors. Note, the model STORM only provides data for 2050. Each plot shows a normalized probability distribution with an integral sum of 1. The x-axis is truncated in some figures, potentially influencing the interpretation of distribution tails, particularly for the MIT hazard-based results.

Supplementary Discussion

We investigate and discuss the role of the two distinctly different moisture variables used in the tropical cyclone genesis index (TCGI) component of CHAZ, which modulate the resulting CHAZ hazard frequency (33). Specifically, event sets generated using column-integral relative humidity (CRH) (82) as a moisture variable show an increase in TC frequencies in a warming climate, whereas those based on saturation deficit (SD) (83) indicate a decrease (Supplementary Figure 8). Despite this distinct divergence in TC frequencies, similar variations are not observed in the TC risk changes when using CHAZ (Supplementary Figures 6 and 7). Furthermore, the sensitivity indices for the TCGI variable are not the highest (Fig. 4 (main text)). On the other hand, events generated using both CRH and SD as moisture variables offer comparable TC risk change estimates, although CRH-TCGI-based hazard sets generally exhibit higher maxima (Supplementary Figures 6 and 7).

This smaller impact of TCGI on risk estimates, in contrast to its evident role in hazard frequency, can be attributed to CHAZ hazard intensity. In this aspect, the choice of GCM exerts a more substantial influence than the TCGI moisture variable (Supplementary Figure 9). Given these insights, we argue that TCGI selection may be of secondary importance in a risk modelling context, especially when socio-economic and exposure-related uncertainties are more pronounced. Nonetheless, using both TCGI versions is advisable to avert possible blind spots in representing future TC risks. Regarding model refinement, both the choice of TCGI and GCM remain critical aspects of epistemic uncertainty that warrant further investigation.

Supplementary Table 1. Maximum kernel density of TC risk change uncertainty distribution. Maximum kernel density estimation of TC risk change uncertainty distribution for estimated change in expected annual damage (EAD) and 100-yr event (rp100) across study regions (North Atlantic/Eastern Pacific (AP), North Indian Ocean (IO), Southern Hemisphere (SH), and North Western Pacific (WP)) for the years 2050 and 2090 and the four models (MIT, CHAZ, STORM, IBTrACS_p). The full uncertainty distribution is shown in Fig. 3 (main text) and Supplementary Figure 2.

region	year	model	Δ EAD (%)	Δ rp100 (%)
AP	2050	MIT	1.63	1.23
		CHAZ	0.80	0.76
		STORM	1.27	1.13
		IBTrACS_p	1.18	0.97
	2090	MIT	3.39	2.41
		CHAZ	1.32	1.16
		STORM	N/A	N/A
		IBTrACS_p	2.40	2.06
IO	2050	MIT	2.76	2.75
		CHAZ	1.80	1.97
		STORM	1.45	1.23
		IBTrACS_p	1.74	2.19
	2090	MIT	10.00	9.04
		CHAZ	2.84	2.95
		STORM	N/A	N/A
		IBTrACS_p	4.03	4.20
SH	2050	MIT	1.84	2.34
		CHAZ	1.03	0.86
		STORM	3.00	1.91
		IBTrACS_p	0.73	0.99
	2090	MIT	6.06	6.16
		CHAZ	1.58	1.71
		STORM	N/A	N/A
		IBTrACS_p	1.81	2.48
WP	2050	MIT	2.36	1.74
		CHAZ	1.29	1.27
		STORM	2.67	2.10
		IBTrACS_p	1.31	1.57
	2090	MIT	4.99	3.88
		CHAZ	1.35	1.65
		STORM	N/A	N/A
		IBTrACS_p	1.91	1.92

Supplementary Fig. 3. Total-order sensitivity indices of future TC risk change across hazard models. Total-order Sobol sensitivity indices for future (2050, 2090) TC risk change calculated with the four models (MIT, CHAZ, STORM, IBTrACS_p), expressed as %-change in expected annual damage (EAD; upper bar) and 100-yr event values (RP 100; lower bar) over the four study regions (North Atlantic/Eastern Pacific (AP), North Indian Ocean (IO), Southern Hemisphere (SH), and North Western Pacific (WP)) and all input factors (different colors); *Vulnerability func. midp.* describes the impact function; *Wind model*; *GCM*, *SSP hazard*, *TCGI moisture variable*, *Event subsampling base*, *Event subsampling future* pertain to the hazard component; *GDP model*; *SSP exposure*, *Exposure urban/rural weighting* relate to the exposure. Note that STORM results are only available for 2050.

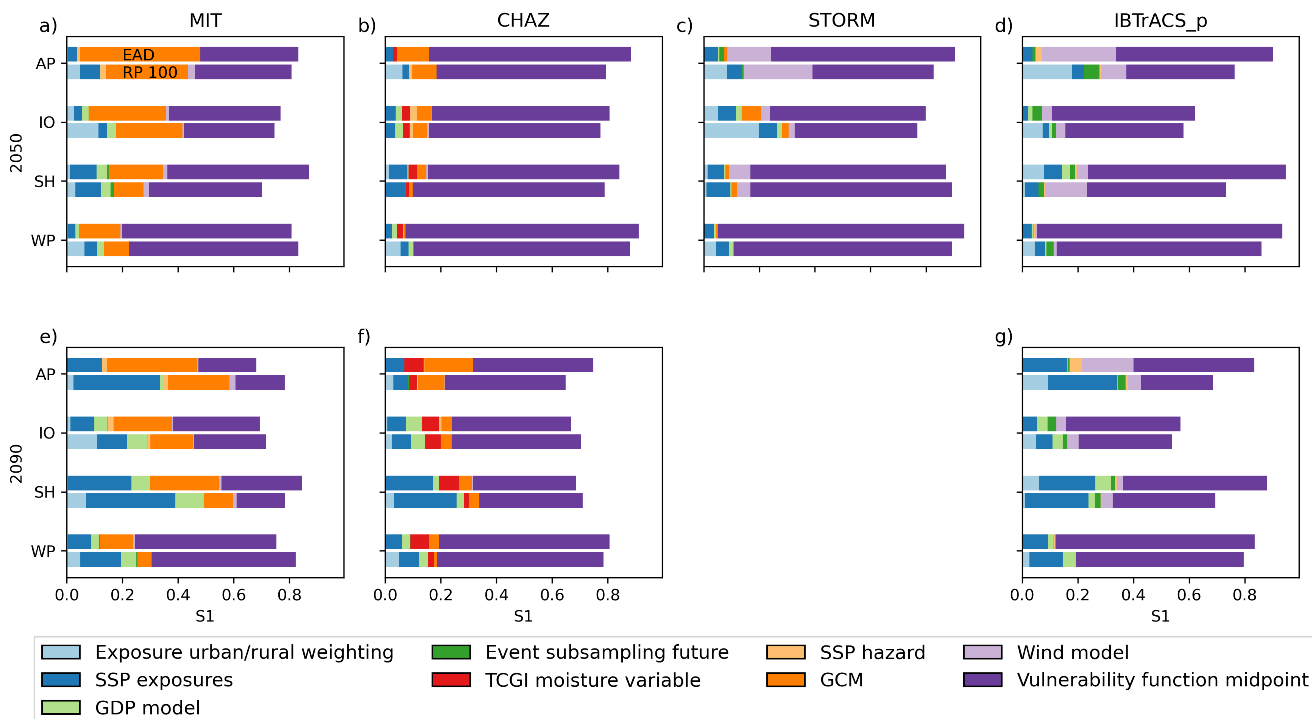

Supplementary Fig. 4. First-order sensitivity indices of absolute future TC risk across hazard models. First-order Sobol sensitivity indices for future (2050, 2090) TC risk calculated with the four models (MIT, CHAZ, STORM, IBTrACS_p), expressed as absolute (calculated in USD) expected annual damage (EAD; upper bar) and 100-yr event values (RP 100; lower bar) over the four study regions (North Atlantic/Eastern Pacific (AP), North Indian Ocean (IO), Southern Hemisphere (SH), and North Western Pacific (WP) and all input factors (different colors); *Vulnerability func. midp.* describes the impact function; *Wind model*; *GCM*, *SSP hazard*, *TCGI moisture variable*, *Event subsampling base*, *Event subsampling future* pertain to the hazard component; *GDP model*; *SSP exposure*, *Exposure urban/rural weighting* relate to the exposure. Note that STORM results are only available for 2050.

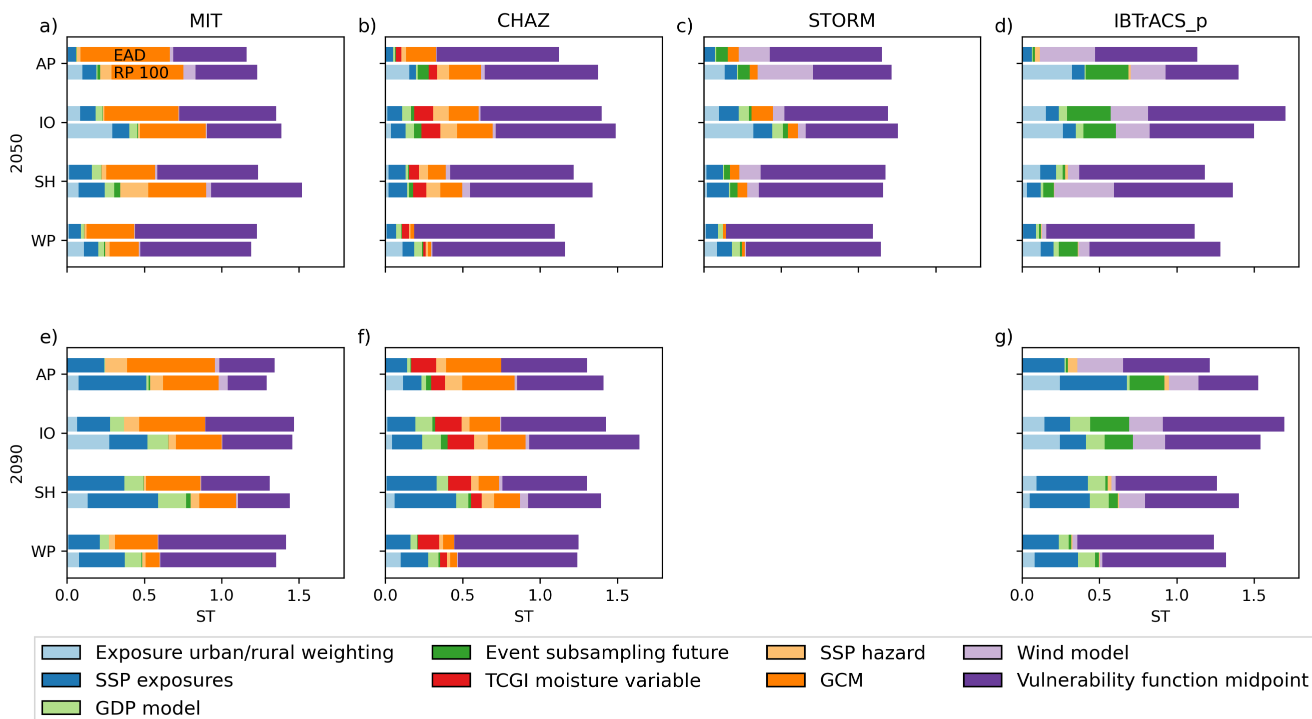

Supplementary Fig. 5. Total-order sensitivity indices of absolute future TC risk across hazard models. Total-order Sobol sensitivity indices for future (2050, 2090) TC risk calculated with the four models (MIT, CHAZ, STORM, IBTrACS_p), expressed as absolute (calculated in USD) expected annual damage (EAD; upper bar) and 100-yr event values (RP 100; lower bar) over the four study regions (North Atlantic/Eastern Pacific (AP), North Indian Ocean (IO), Southern Hemisphere (SH), and North Western Pacific (WP) and all input factors (different colors); *Vulnerability func. midp.* describes the impact function; *Wind model*; *GCM*, *SSP hazard*, *TCGI moisture variable*, *Event subsampling base*, *Event subsampling future* pertain to the hazard component; *GDP model*; *SSP exposure*, *Exposure urban/rural weighting* relate to the exposure. Note that STORM results are only available for 2050.

Supplementary Table 2. Largest sensitivity indices for future TC risk change estimates. Highest first- (S1) and total-order (ST) Sobol sensitivity indices for both risk change metrics (expected annual damage (EAD) and 100-yr event (rp100)), expressed as %-change in the four study regions (North Atlantic/Eastern Pacific (AP), North Indian Ocean (IO), Southern Hemisphere (SH), and North Western Pacific (WP) for both future periods (2050, 2090) and all four models (MIT, CHAZ, STORM, IBTrACS_p. Indices colored blue pertain to the hazard component (*GCM, Event subsampling base/future, TCGI*), green to the exposure (*SSP exposure, GDP model*) and red to the impact function (*Vulnerability func. midp.*). Plots showing all sensitivity indices can be found in Fig. 4 (main text) and Supplementary Figure 3.

region	year	model	S1 EAD	S1 rp100	ST EAD	ST rp100
AP	2050	MIT	GCM	GCM	GCM	GCM
		CHAZ	GCM	GCM	GCM	GCM
		STORM	SSP exposure	SSP exposure	GCM	SSP exposure
		IBTrACS_p	SSP exposure	Event subsampling base	SSP exposure	Event subsampling base
	2090	MIT	GCM	GCM	GCM	GCM
		CHAZ	GCM	SSP exposure	GCM	GCM
		STORM	N/A	N/A	N/A	N/A
		IBTrACS_p	SSP exposure	SSP exposure	SSP exposure	SSP exposure
IO	2050	MIT	GCM	GCM	GCM	GCM
		CHAZ	GCM	GCM	GCM	GCM
		STORM	GCM	SSP exposure	GCM	SSP exposure
		IBTrACS_p	Event subsampling future	Event subsampling base	Event subsampling base	Event subsampling base
	2090	MIT	GCM	GCM	GCM	GCM
		CHAZ	GCM	TCGI moisture var.	GCM	GCM
		STORM	N/A	N/A	N/A	N/A
		IBTrACS_p	Event subsampling future	Event subsampling base	Event subsampling base	Event subsampling base
SH	2050	MIT	GCM	GCM	GCM	GCM
		CHAZ	SSP exposure	SSP exposure	GCM	GCM
		STORM	SSP exposure	SSP exposure	SSP exposure	Vulnerability func. midp.
		IBTrACS_p	SSP exposure	SSP exposure	GDP model	GDP model
	2090	MIT	GCM	SSP exposure	GCM	GCM
		CHAZ	SSP exposure	SSP exposure	SSP exposure	SSP exposure
		STORM	N/A	N/A	N/A	N/A
		IBTrACS_p	SSP exposure	SSP exposure	SSP exposure	SSP exposure
WP	2050	MIT	GCM	GCM	GCM	GCM
		CHAZ	SSP exposure	SSP exposure	SSP exposure	SSP exposure
		STORM	SSP exposure	SSP exposure	SSP exposure	SSP exposure
		IBTrACS_p	SSP exposure	Event subsampling base	SSP exposure	Event subsampling base
	2090	MIT	GCM	GCM	GCM	GCM
		CHAZ	SSP exposure	SSP exposure	SSP exposure	SSP exposure
		STORM	N/A	N/A	N/A	N/A
		IBTrACS_p	SSP exposure	SSP exposure	SSP exposure	Event subsampling base

Supplementary Table 3. Largest sensitivity indices for future TC risk estimates. Highest first- (S1) and total-order (ST) Sobol sensitivity indices for both risk metrics (expected annual damage (EAD) and 100-yr event (rp100)), expressed in absolute values (USD) in the four study regions (North Atlantic/Eastern Pacific (AP), North Indian Ocean (IO), Southern Hemisphere (SH), and North Western Pacific (WP) for both future periods (2050, 2090) and all four models (MIT, CHAZ, STORM, IBTrACS_p. Indices colored blue pertain to the hazard component (*GCM*), green to the exposure (*SSP exposure*) and red to the impact function (*Vulnerability func. midp.*). Plots showing all sensitivity indices can be found in Supplementary Figure 4 and 5.

region	year	model	S1 EAD	S1 rp100	ST EAD	ST rp100
AP	2050	MIT	GCM	GCM	GCM	GCM
		CHAZ	Vulnerability func. midp.	Vulnerability func. midp.	Vulnerability func. midp.	Vulnerability func. midp.
		STORM	Vulnerability func. midp.	Vulnerability func. midp.	Vulnerability func. midp.	Vulnerability func. midp.
		IBTrACS_p	Vulnerability func. midp.	Vulnerability func. midp.	Vulnerability func. midp.	Vulnerability func. midp.
	2090	MIT	GCM	SSP exposure	GCM	SSP exposure
		CHAZ	Vulnerability func. midp.	Vulnerability func. midp.	Vulnerability func. midp.	Vulnerability func. midp.
		STORM	N/A	N/A	N/A	N/A
		IBTrACS_p	Vulnerability func. midp.	Vulnerability func. midp.	Vulnerability func. midp.	SSP exposure
IO	2050	MIT	Vulnerability func. midp.	Vulnerability func. midp.	Vulnerability func. midp.	Vulnerability func. midp.
		CHAZ	Vulnerability func. midp.	Vulnerability func. midp.	Vulnerability func. midp.	Vulnerability func. midp.
		STORM	Vulnerability func. midp.	Vulnerability func. midp.	Vulnerability func. midp.	Vulnerability func. midp.
		IBTrACS_p	Vulnerability func. midp.	Vulnerability func. midp.	Vulnerability func. midp.	Vulnerability func. midp.
	2090	MIT	Vulnerability func. midp.	Vulnerability func. midp.	Vulnerability func. midp.	Vulnerability func. midp.
		CHAZ	Vulnerability func. midp.	Vulnerability func. midp.	Vulnerability func. midp.	Vulnerability func. midp.
		STORM	N/A	N/A	N/A	N/A
		IBTrACS_p	Vulnerability func. midp.	Vulnerability func. midp.	Vulnerability func. midp.	Vulnerability func. midp.
SH	2050	MIT	Vulnerability func. midp.	Vulnerability func. midp.	Vulnerability func. midp.	Vulnerability func. midp.
		CHAZ	Vulnerability func. midp.	Vulnerability func. midp.	Vulnerability func. midp.	Vulnerability func. midp.
		STORM	Vulnerability func. midp.	Vulnerability func. midp.	Vulnerability func. midp.	Vulnerability func. midp.
		IBTrACS_p	Vulnerability func. midp.	Vulnerability func. midp.	Vulnerability func. midp.	Vulnerability func. midp.
	2090	MIT	Vulnerability func. midp.	SSP exposure	Vulnerability func. midp.	SSP exposure
		CHAZ	Vulnerability func. midp.	Vulnerability func. midp.	Vulnerability func. midp.	Vulnerability func. midp.
		STORM	N/A	N/A	N/A	N/A
		IBTrACS_p	Vulnerability func. midp.	Vulnerability func. midp.	Vulnerability func. midp.	Vulnerability func. midp.
WP	2050	MIT	Vulnerability func. midp.	Vulnerability func. midp.	Vulnerability func. midp.	Vulnerability func. midp.
		CHAZ	Vulnerability func. midp.	Vulnerability func. midp.	Vulnerability func. midp.	Vulnerability func. midp.
		STORM	Vulnerability func. midp.	Vulnerability func. midp.	Vulnerability func. midp.	Vulnerability func. midp.
		IBTrACS_p	Vulnerability func. midp.	Vulnerability func. midp.	Vulnerability func. midp.	Vulnerability func. midp.
	2090	MIT	Vulnerability func. midp.	Vulnerability func. midp.	Vulnerability func. midp.	Vulnerability func. midp.
		CHAZ	Vulnerability func. midp.	Vulnerability func. midp.	Vulnerability func. midp.	Vulnerability func. midp.
		STORM	N/A	N/A	N/A	N/A
		IBTrACS_p	Vulnerability func. midp.	Vulnerability func. midp.	Vulnerability func. midp.	Vulnerability func. midp.

Supplementary Table 4. List of CMIP6 models used in the downscaling of tropical cyclone event sets.

Institution	Model	Short name	Source
National Center for Atmospheric Research	CESM2	CESM2	Danabasoglu et al. (2020) (72)
Centre National de Recherches Météorologiques	CNRM-CM6-1	CNRM6	Voldoire et al. (2019) (73)
EC-Earth consortium	EC-Earth3	ECEARTH	EC-Earth Consortium (2019) (74)
Institute of Atmospheric Physics, Chinese Academy of Sciences	FGOALS-g3	FGOALS	Li et al. (2019) (75)
Institut Pierre Simon Laplace	IPSL-CM6A-LR	IPSL6	Hourdin et al. (2016) (76)
Japan Agency for Marine-Earth Science and Technology	MIROC6	MIROC6	Tatebe et al. (2019) (77)
Max Planck Institute	MPI-ESM1-2-HR	MPI2	Müller et al. (2018) (78)
Meteorological Research Institute, Tsukuba, Japan	MRI6-ESM2-0	MRI6	Yukimoto et al. (2019) (79)
United Kingdom Met Office	UKESM1-0-LL	UKMO6	Sellar et al. (2020) (80)

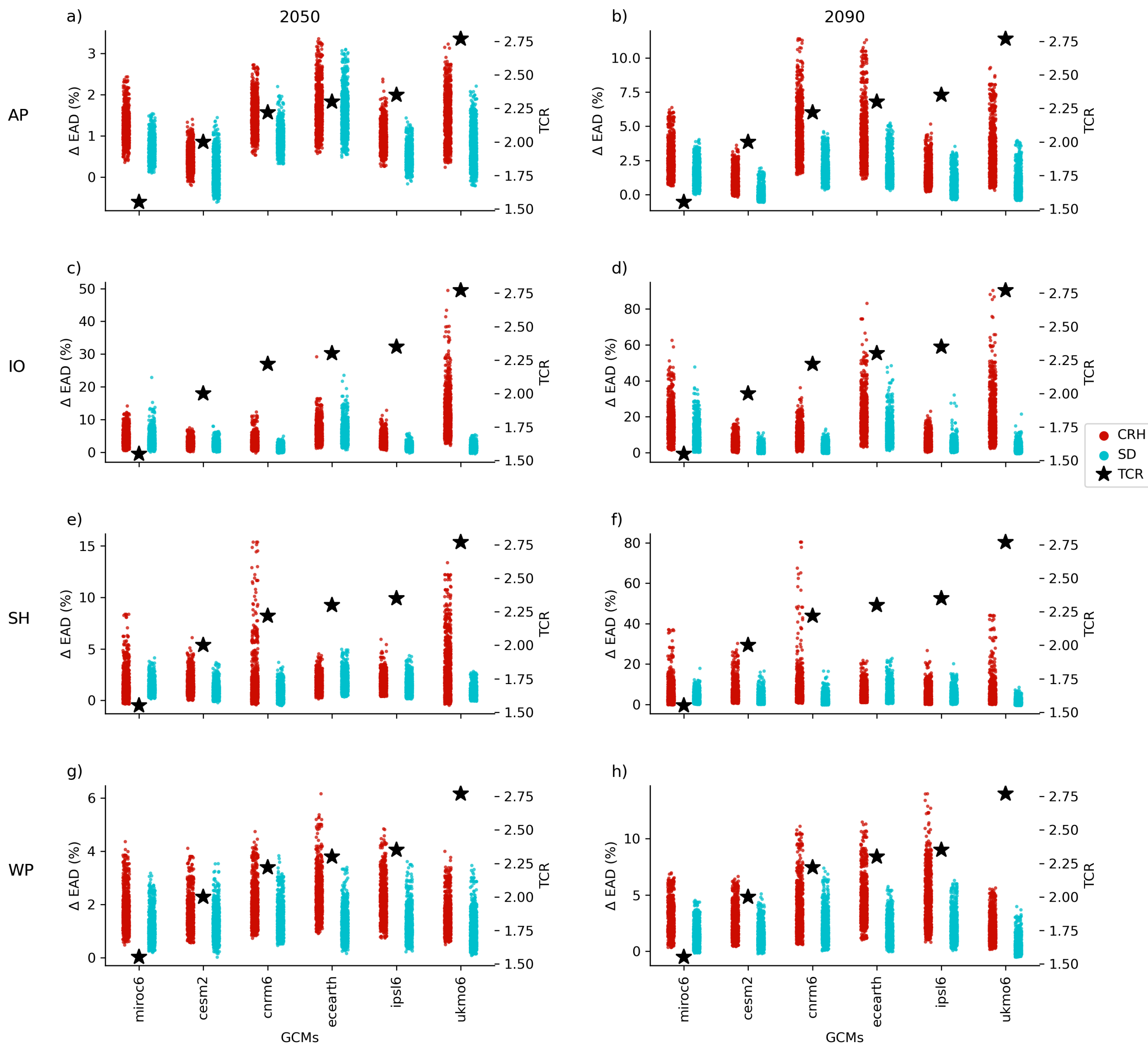

Supplementary Fig. 6. EAD change in CHAZ apportioned to GCMs and TCGI variables. Model simulations of the expected annual damage (EAD) change by 2050 (a, c, e, g) and 2090 (b, d, f, h) attributed to the six GCMs and two moisture variables used in the TCGI underlying the CHAZ TC hazard sets. GCMs are ordered by increasing transient climate response (TCR) values (Supplementary Table 5), which are shown as black stars on a secondary y-axis. Results are shown over the four study regions North Atlantic/Eastern Pacific (AP), North Indian Ocean (IO), Southern Hemisphere (SH), and North Western Pacific (WP).

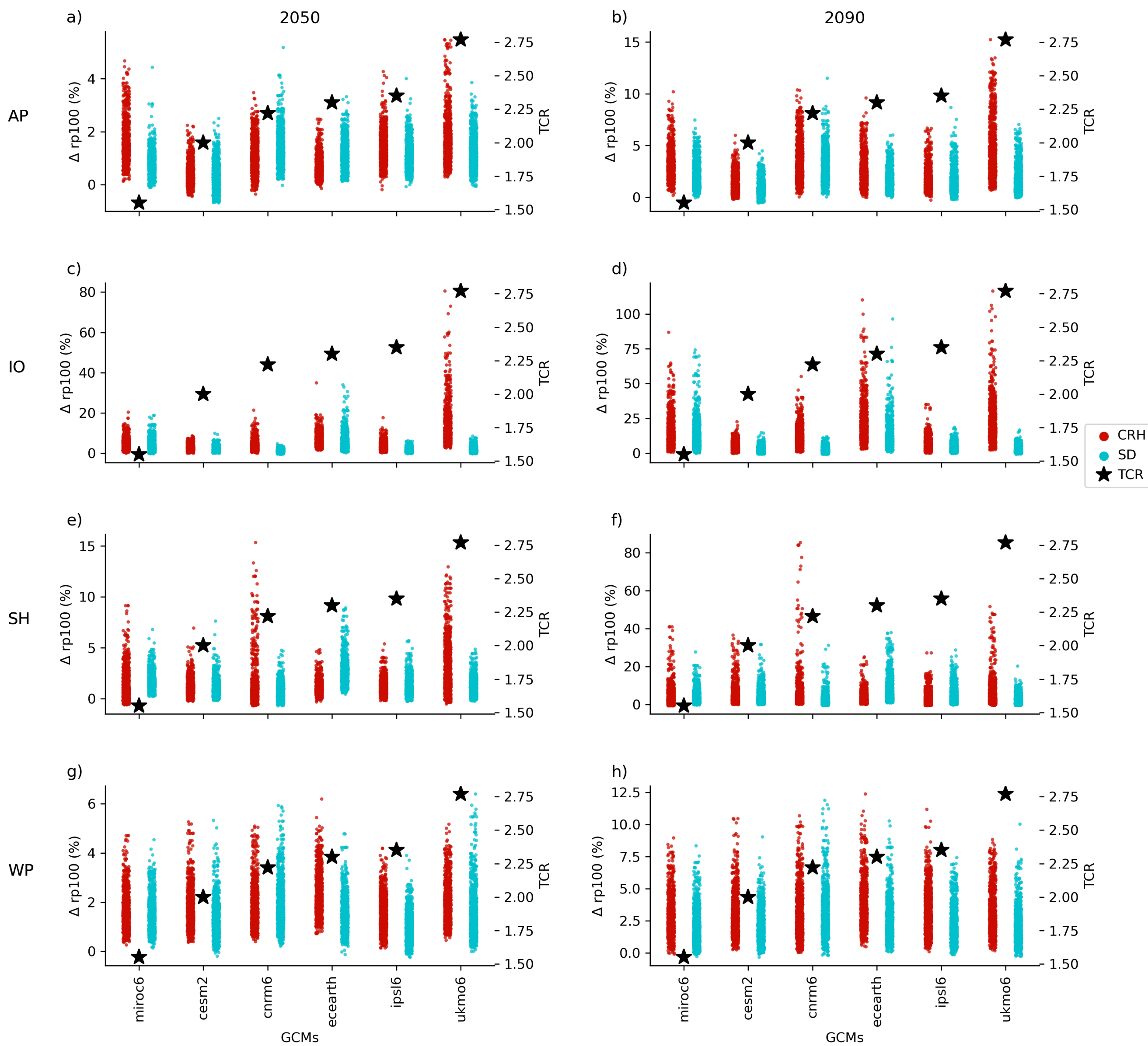

Supplementary Fig. 7. RP100 change in CHAZ apportioned to GCMs and TCGI variables. Model simulations of the 100-yr event (rp100) change by 2050 (a, c, e, g) and 2090 (b, d, f, h) attributed to the six GCMs and two moisture variables used in the TCGI underlying the CHAZ TC hazard sets. GCMs are ordered by increasing transient climate response (TCR) values (Supplementary Table 5), which are shown as black stars on a secondary y-axis. Results are shown over the four study regions North Atlantic/Eastern Pacific (AP), North Indian Ocean (IO), Southern Hemisphere (SH), and North Western Pacific (WP).

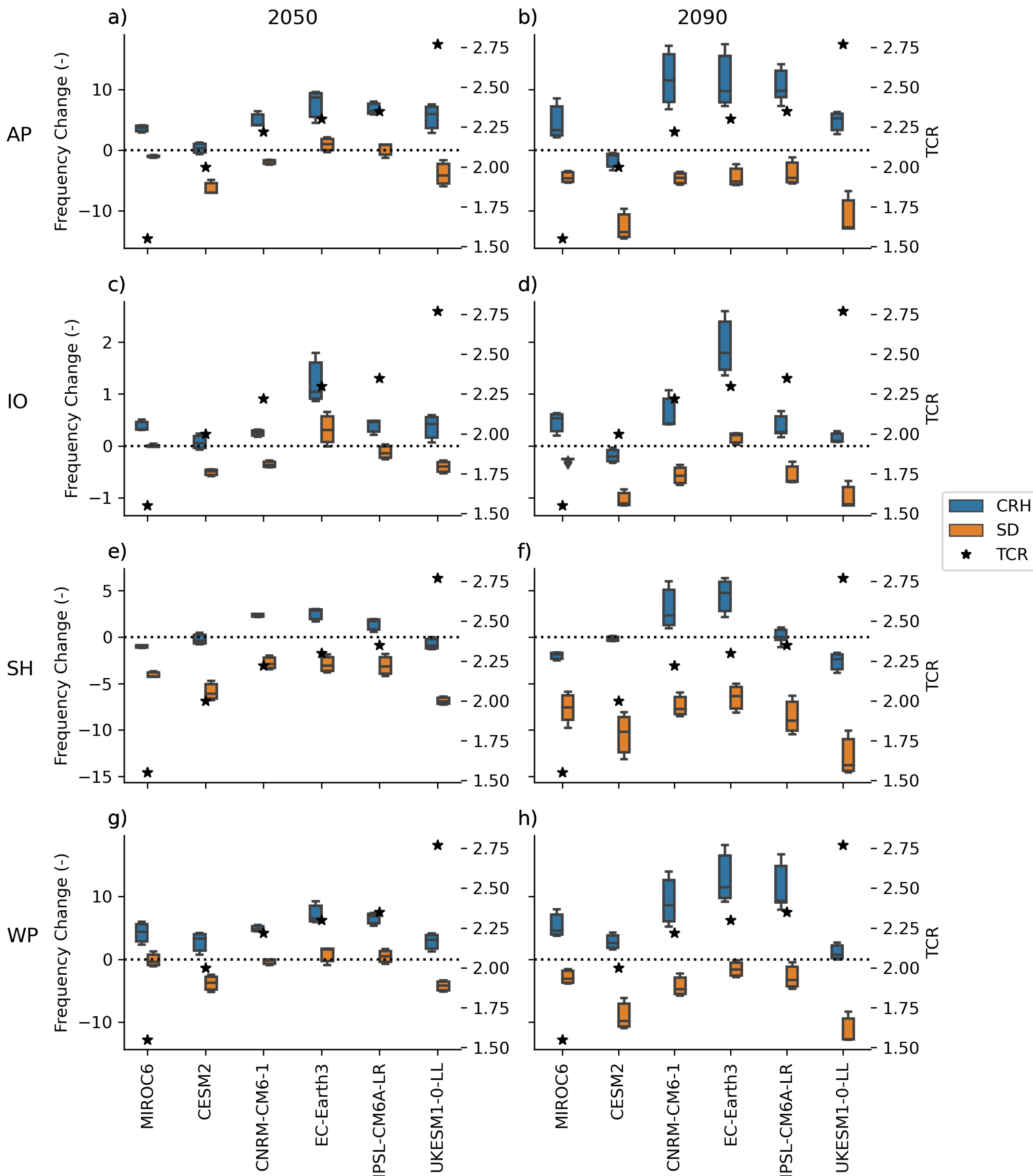

Supplementary Fig. 8. Frequency changes in CHAZ hazard sets. CHAZ hazard frequency change values for event sets of the six different GCMs, separated by the two TCGI moisture variables (CRH, SD) and shown for two future time periods (2050, 2090) and four study regions North Atlantic/Eastern Pacific (AP), North Indian Ocean (IO), Southern Hemisphere (SH), and North Western Pacific (WP). Frequency change values were calculated relative to the historical period and analyzed for the full event set, hence not limited to land-influencing storms. Additionally, transient climate response (TCR) values for the six GCMs are shown on a secondary y-axis (see Supplementary Table 5).

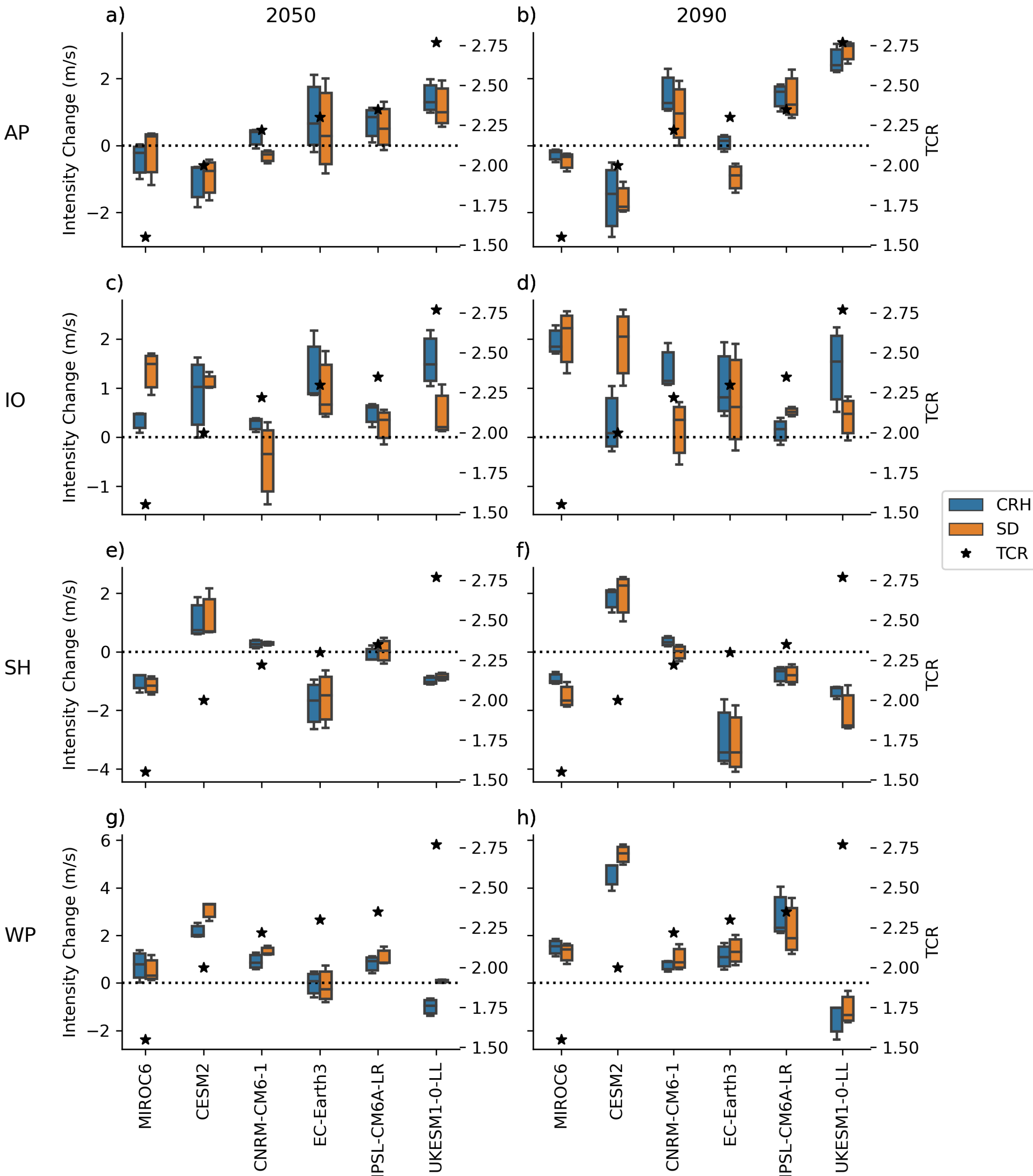

Supplementary Fig. 9. Intensity changes in CHAZ hazard sets. CHAZ hazard intensity change values for event sets of the six different GCMs, separated by the two TCGI moisture variables (CRH, SD) and shown for two future time periods (2050, 2090) and four study regions North Atlantic/Eastern Pacific (AP), North Indian Ocean (IO), Southern Hemisphere (SH), and North Western Pacific (WP). Intensity change values were derived for both wind models used in the hazard generation (60, 71). Intensity changes are calculated as the mean over the maximum sustained wind speeds of all TCs in the future event sets minus the equivalent of the historical period. Note, we analyze the full event set and do not limit the analysis to land-influencing storms. Additionally, transient climate response (TCR) values for the six GCMs are shown on a secondary y-axis (see Supplementary Table 5).

Supplementary Table 5. Transient climate response (TCR) and equilibrium climate sensitivity (ECS) values for the nine GCMs, including a screen if the models fall into the likely range of projected TCR or ECS. Values are obtained from Hausfather et al. (2022) (81) supplementary data.

Model	TCR	TCR screen (likely)	ECS150	ECS130	ECS screen (likely)
CESM2	2.00	yes	5.15	6.43	no
CNRM-CM6-1	2.22	no	4.90	4.76	no
EC-Earth3	2.30	no	4.26	N/A	no
FGOALS-g3	1.50	yes	2.87	3.10	yes
IPSL-CM6A-LR	2.35	no	4.70	5.18	no
MIROC6	1.55	yes	2.60	2.59	yes
MPI-ESM1-2-HR	1.64	yes	2.98	3.34	yes
MRI6-ESM2-0	1.67	yes	3.13	3.42	yes
UKESM1-0-LL	2.77	no	5.36	5.49	no